C.2

Interaction Notes

Note 259

August 1974

Transient Characterization of Circular Loop Using Singularity Expansion Method

K.R. Umashankar and D.R. Wilton
University of Mississippi
University, Mississippi

Abstract

Using the singularity expansion method a circular loop structure is characterized and its current response is given treating it both as an antenna and as a scatterer in free space. The extension of the solution for dissipative medium is also discussed.

SINGULARITY EXPANSION OF CIRCULAR LOOP ANTENNA

A circular loop structure is characterized using SEM to treat a loop antenna and scatterer in free space. Because of the rotational symmetry of the circular loop, a Pocklington type or E-field integral equation can be formulated and approximately solved using a Fourier series representation for the current induced as discussed by Wu [1]. The loop structure happens to be an important case for SEM analysis, wherein the choice of Fourier series for the current representation diagonalizes the matrix corresponding to the integral operator and hence simutaneously demonstrates that the current basis functions are the modal currents. The fact that the modal currents are all of the form $\exp(jn\phi)$ makes it possible to tabulate once and for all, for various loop sizes, simply the resonant frequencies of oscillation and the corresponding residues which are the basic SEM characteristic results for constructing either the frequency or the time domain solution.

As will be demonstrated, the method of analysis can be conveniently extended to the case of a circular loop in a dissipative medium without re-solving the original problem again.

1. Integral equation for the circular loop

Assuming an e^{st} time dependence, an integral equation of the

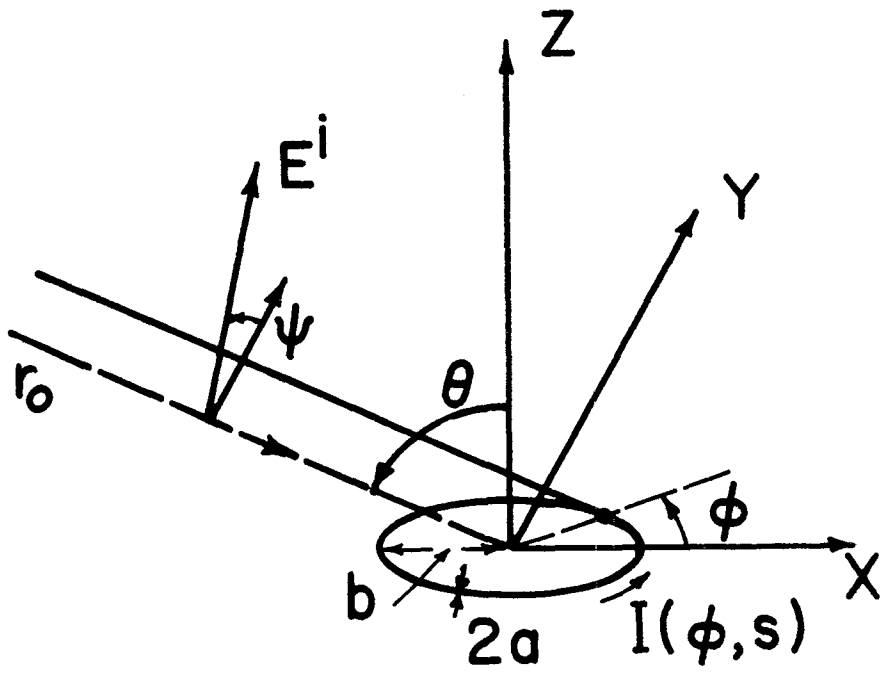

Figure 1 Geometry of the circular loop.

Pocklington E-field type for the current $I(\phi,s)$ induced on the circular loop is formulated in an infinite isotropic homogeneous medium of permeability μ, permittivity ε, and conductivity σ_c. The loop structure is in the xy plane with the z axis coinciding with its center, Figure 1, and has a loop radius b and wire cross sectional radius a. Based on thin wire assumptions

$$a^2 << b^2, \quad |\tfrac{s}{c}a| << 1 \tag{1}$$

If $E^i_\phi(\phi,s)$ is the tangential component of the incident electric field on the surface of the perfectly conducting circular loop, then an integral equation for the current induced $I(\phi,s)$ on the circular loop [2] is given by

$$bE^i_\phi(\phi,s) = \frac{j\xi}{4\pi}\int_{-\pi}^{+\pi} M(\phi-\phi',s)I(\phi',s)d\phi' \tag{2}$$

where the kernel function

$$M(\phi-\phi',s) = \left[\frac{1}{-j\gamma b}\frac{\partial^2}{\partial\phi^2} - j\gamma b\cos(\phi-\phi')\right]W(\phi-\phi',\gamma) \tag{3}$$

$$W(\phi-\phi',\gamma) = \frac{b}{2\pi}\int_{-\pi}^{+\pi}\frac{e^{-\gamma R}}{R}d\psi \tag{4}$$

$$\gamma = \alpha + j\beta = [\mu s(\varepsilon s + \sigma_c)]^{\frac{1}{2}} \tag{5}$$

$$R^2 = [2b\sin\tfrac{\phi-\phi'}{2}]^2 + [2a\sin\tfrac{\psi}{2}]^2 \tag{6}$$

and

$$\xi = \left[\frac{s\mu}{(s\varepsilon + \sigma_c)}\right]^{\frac{1}{2}} \tag{7}$$

The integral eqution (2) for the current on the circular loop could, of course, be solved using the method of moments and SEM used to characterize the circular loop structure as has been done for the circular cylinder and the L-wire strucutres. But the rotational symmetry of the loop makes it expedient to expand the kernel function $M(\phi-\phi',s)$ and the current distribution $I(\phi',s)$ in Fourier series and with an appropriate choice of weighting functions, hence we write the following Fourier series expansions

$$M(\phi-\phi',s) = \sum_{n=-\infty}^{+\infty} a_n(s)e^{-jn(\phi-\phi')} \tag{8}$$

$$I(\phi',s) = \sum_{n=-\infty}^{+\infty} I_n(s)e^{-jn\phi'} \tag{9}$$

Substituting (8) and (9) into the integral equation (2), we obtain

$$bE_\phi^i(\phi,s) = \frac{j\xi}{2}\sum_{n=-\infty}^{+\infty} a_n(s)I_n(s)e^{-jn\phi} \tag{10}$$

and finally

$$a_n(s)I_n(s) = \frac{-j}{\xi\pi}\int_{-\pi}^{+\pi} bE_\phi^i(\phi,s)e^{jn\phi}d\phi \tag{11}$$

where the Fourier coefficients

$$a_n(s) = a_{-n}(s) = \frac{-j\gamma b}{2}\left[K_{n+1} + K_{n-1}\right] + \frac{n^2}{j\gamma b} K_n \tag{12}$$

For a thin wire loop, the coefficients K_n are given by

$$K_0 = \frac{1}{\pi} \ell n \frac{8b}{a} - \frac{1}{2} \int_0^{-j2\gamma b} [\Omega_0(z) + j\, J_0(z)]dz \tag{13}$$

$$K_{n+1} = K_n + \Delta_n, \quad K_n = K_{-n} \tag{14}$$

$$\Delta_n = \Omega_{2n+1}(-j2\gamma b) + J_{2n+1}(-j2\gamma b) \tag{15}$$

where $J_{2n+1}(z)$ and $\Omega_{2n+1}(z)$ are the complex Bessel and the Lommel-Weber functions respectively of order $(2n + 1)$.

Further the incident field is also expanded in a Fourier series

$$E^i_\phi(\phi,s) = \sum_{n=-\infty}^{+\infty} E^i_{\phi n}(s) e^{-jn\phi} \tag{16}$$

Comparison with (10) and observing the orthogonality of the functions $\exp(-jn\phi)$ permits us to write

$$I_n(s) = \frac{-j\ 2b}{\xi} \frac{E^i_{\phi n}(s)}{a_n(s)} \tag{17}$$

Assuming that each of the functions $a_n(s)$ has distinct zeros, we conclude from (9) that the spatial dependence of each natural mode (corresponding to a zero of $a_n(s)$) is of the form $\exp(-jn\phi)$. It is

convenient to view the function $1/a_n(s)$ as a transfer function which relates the output $I_n(s)$ to input $E^i_{\phi n}(s)$.

For an antenna problem, the coefficients of the current distribution on the circular loop structure corresponding to a delta-gap excitation at $\phi = 0$, Figure 2, are simply

$$E^i_{\phi n}(s) = \frac{V_0(s)}{2\pi b} \tag{18}$$

and hence the current coefficients are

$$I_n(s) = \frac{-jV_0(s)}{\xi\pi} \frac{1}{a_n(s)} \tag{19}$$

For a scattering problem excited by an incident plane wave traveling along the direction r_0, ϕ_0, and making an angle θ with the z axis, Figure 1,

$$E^i_{\phi n}(s) = E^i_0(s)\ f_n(s) \tag{20}$$

where $E^i_0(s)$ is the incident field term referred to the center of the loop and

$$f_n(s) = j^{n-1} \cos\psi\ e^{-jn\phi_0} J'_n(-j\gamma b \sin\theta) + j^n \sin\psi \cos\theta\ e^{-jn\phi_0} \frac{nJ_n(-j\gamma b \sin\theta)}{-j\gamma b \sin\theta} \tag{21}$$

On substituting (20) into the equation (16), the coefficients $I_n(s)$ of the current distribution on the circular loop scatterer can

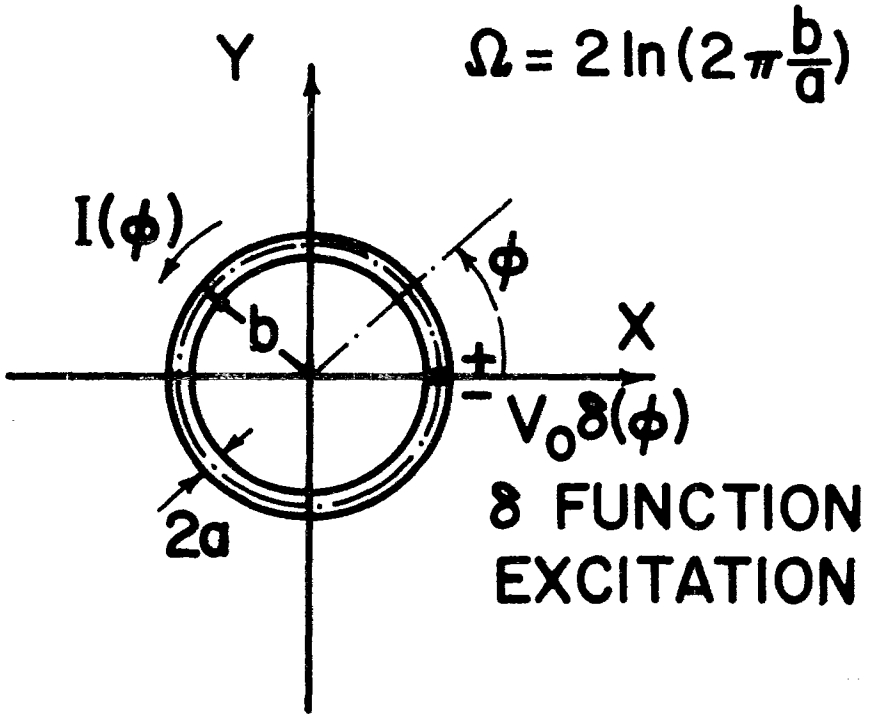

Figure 2 Geometry of circular loop antenna.

be obtained by (11), which yields

$$I_n(s) = \frac{-j2b}{\xi} E_0^i(s) \frac{f_n(s)}{a_n(s)} \tag{22}$$

2 Application of SEM to the circular loop antenna in lossless free space

The induced current distribution $I(\phi,s)$ on the circular loop antenna structure, Figure 2, corresponding to the delta-gap input excitation is given by equations (9) and (19)

$$I(\phi,s) = \frac{-jV_0(s)}{\eta\pi} \sum_{n=-\infty}^{+\infty} \frac{e^{-jn\phi}}{a_n(s)} \tag{23}$$

where in the equation (19), $\gamma = s/c$ and $\xi = \eta$ are substituted for the lossless free space medium and

$$\eta = [\mu/\epsilon]^{\frac{1}{2}} = 120\pi \tag{24}$$

The expression (23) is in a form suitable for SEM analysis. Every Fourier coefficient $a_n(s) = 0$ has zeros at $s = s_{ni}$ which are resonant frequencies of oscillation of the circular loop structure and the term $1/a_n(s)$ can be expanded in a residue series (Appendix A and expression 56A)

$$\frac{-j}{a_n(s)} = \sum_i \frac{R_{ni}}{s-s_{ni}} \tag{25}$$

where R_{ni} is the residue of $1/a_n(s)$ at the pole $s = s_{ni}$. Hence for

the circular loop antenna excited by a time-domain delta function input, the expression for the induced current becomes

$$I(\phi,s) = \frac{V_0(s)}{\eta\pi} \sum_n \sum_i \frac{R_{ni}}{s-s_{ni}} e^{-jn\phi} \tag{26}$$

The frequency domain solution corresponding to the time harmonic input voltage $V_0(j\omega)$ is obtained easily by substituting $s = j\omega$ in the equation (26). We should further note that at $\phi = 0$, equation (26) gives the input admittance of the circular loop antenna with delta-gap input excitation. If $G(j\omega)$ and $B(j\omega)$ are the input conductance and susceptance at the delta-gap terminals

$$Y(j\omega) = G(j\omega) + jB(j\omega) = \frac{1}{\eta\pi} \sum_n \sum_i \frac{R_{ni}}{j\omega-s_{ni}} \tag{27}$$

The time domain solution for the current on the circular loop antenna can be obtained by taking the Laplace inverse of the equation (26)

$$i(\phi,t) = \frac{1}{2\pi j} \int_{C_B} \frac{V_0(s)}{\eta\pi} \sum_n \sum_i \frac{R_{ni}}{s-s_{ni}} e^{-jn\phi} e^{st} ds \tag{28}$$

where C_B is the Bromwich contour, Figure 16, in the complex s-plane.

If the antenna gap is excited by a time-domain delta function of strength V_0 at $t = 0$, then

$$E^i_{\phi n} = \frac{V_0}{2\pi b} \tag{29}$$

which is independent of s and we note that the only singularities in the integrand of (28) are the simple poles at $s = s_{ni}$ and they are all located in the left half of complex s plane. Hence closing the contour C_B for $t < 0$ by C_∞^+ in Figure 16, gives zero current response and for $t > 0$, the contour C_B is closed along C_∞^- enclosing all the pole locations in the left half of the complex plane, which results in the time domain current response

$$i(\phi,t) = \frac{V_0}{\eta\pi} \sum_{n=-\infty}^{+\infty} \sum_i R_{ni} e^{s_i t} e^{-jn\phi} u(t) \qquad (30)$$

where u(t) is a Heaviside unit step function. The fact that there must necessarily be a time delay between the time the loop is excited at $\phi = 0$ and the time the response appears at other points on the loop requires that the sum in (30) sums to zero before the excitation reaches the observation point.

For any other general excitation in time at the gap viz., the step function or the pulse function in time with a finite width, the corresponding Laplace transform of $V_0(s)$ is substituted in (28) and the contour integral may be evaluated either directly or by convolving in time with the delta function response.

3. Numerical results for circular loop antenna in free space

In this section the numerical results of the application of SEM to the circular loop antenna in free space are presented. The pole

plots, the pole trajectories, and the residues for the various loop sizes, and the time domain current corresponding to the delta function and the pulse function inputs are given. Since the modal current distributions are all of the form $\exp(jn\phi)$ where n is the mode number, they are not shown here. In the frequency domain, the first few $1/a_n(s)$ Fourier coefficients are constructed corresponding to a time harmonic input excitation. The results of input admittance calculations for the circular loop are omitted here, but are given in the latter section on the circular loop antenna in dissipative medium.

The distribution of the pole locations for the circular loop strucutre shown in Figure 3 is somewhat different from the previous cases analyzed, viz., the circular cylinder and the L-wire strucutres. Furthermore, corresponding to each Fourier mode n, there exists an infinite set of poles. This is in contrast to the other cases considered a unique modal current is associated with each pole.

The pole locations for each mode may be divided into the following three catagories:

i) Roughly, the poles are all located in layers parallel to the $j\omega$-axis. There is a pole very near the $j\omega$-axis at approximately $\omega = n$. This pole is the principal contributor to the time domain response of the loop at late times and the imaginary part of the pole location corresponds closely to a resonant frequency of the loop for an excitation of the form $\exp(j\omega t - jn\phi)$.

ii) There are (n + 1) poles (including conjugate pairs) which lie roughly on the left hand side of an ellipse centered at s = 0 and with

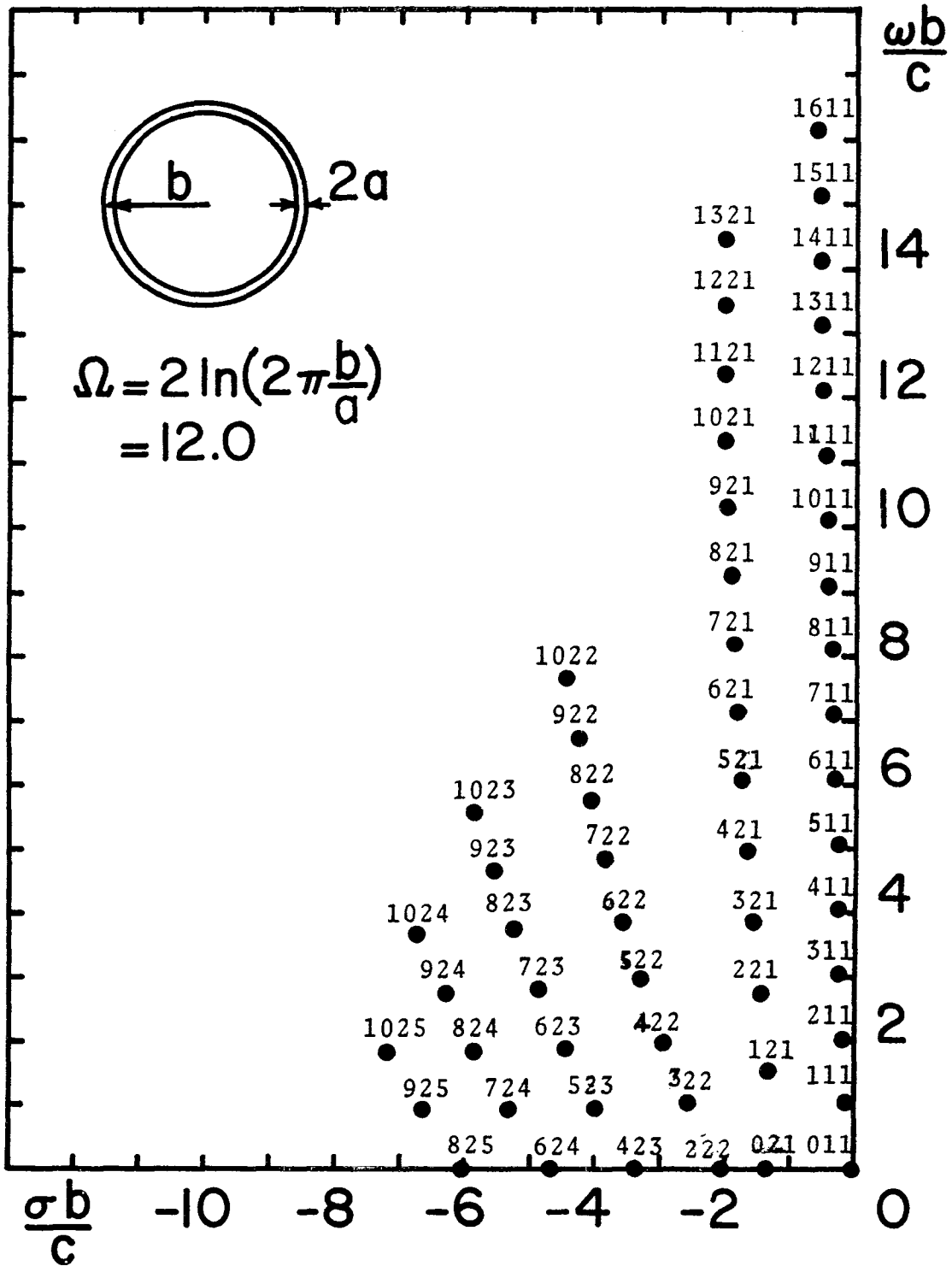

Figure 3 Natural frequencies of the circular loop, $\Omega = 12.0$.

a semi-major axis somewhat larger than n.

iii) There is a third group of poles lying almost parallel to the $j\omega$-axis. This layer contains an infinite number of poles and they are spaced approximately $\Delta\omega = \pi c/b$ units apart.

The pole plot of Figure 3 also shows the indexing scheme used which is summarized as follows:

Pole index: n ℓ p

- n : Mode number of the Fourier coefficients
  0, ± 1, ± 2, ...
- ℓ : 1 type (i) pole
  2 type (ii) pole
  3 type (iii) pole (not shown in figure)
- p : Sets of poles in a layer

There is a simple pole at the origin corresponding to the zeroth mode and every even mode contributes a pole on the negative real axis.

Figure 4 shows all the pole locations of the third mode $a_3(s)$. The layer of poles running parallel to the $j\omega$-axis are infinite in number and are basically the same for all odd modes for large frequencies. Another set of poles for the even modes exists approximately in between those of the odd modes. In Appendix A, a simple asymptotic formula which permits accurate calculation of the locations of these type $\ell = 3$ poles is given.

The plot of the pole trajectories of the principal poles ($\ell = 1$) closest to the $j\omega$-axis are shown in Figure 5 as a function of loop

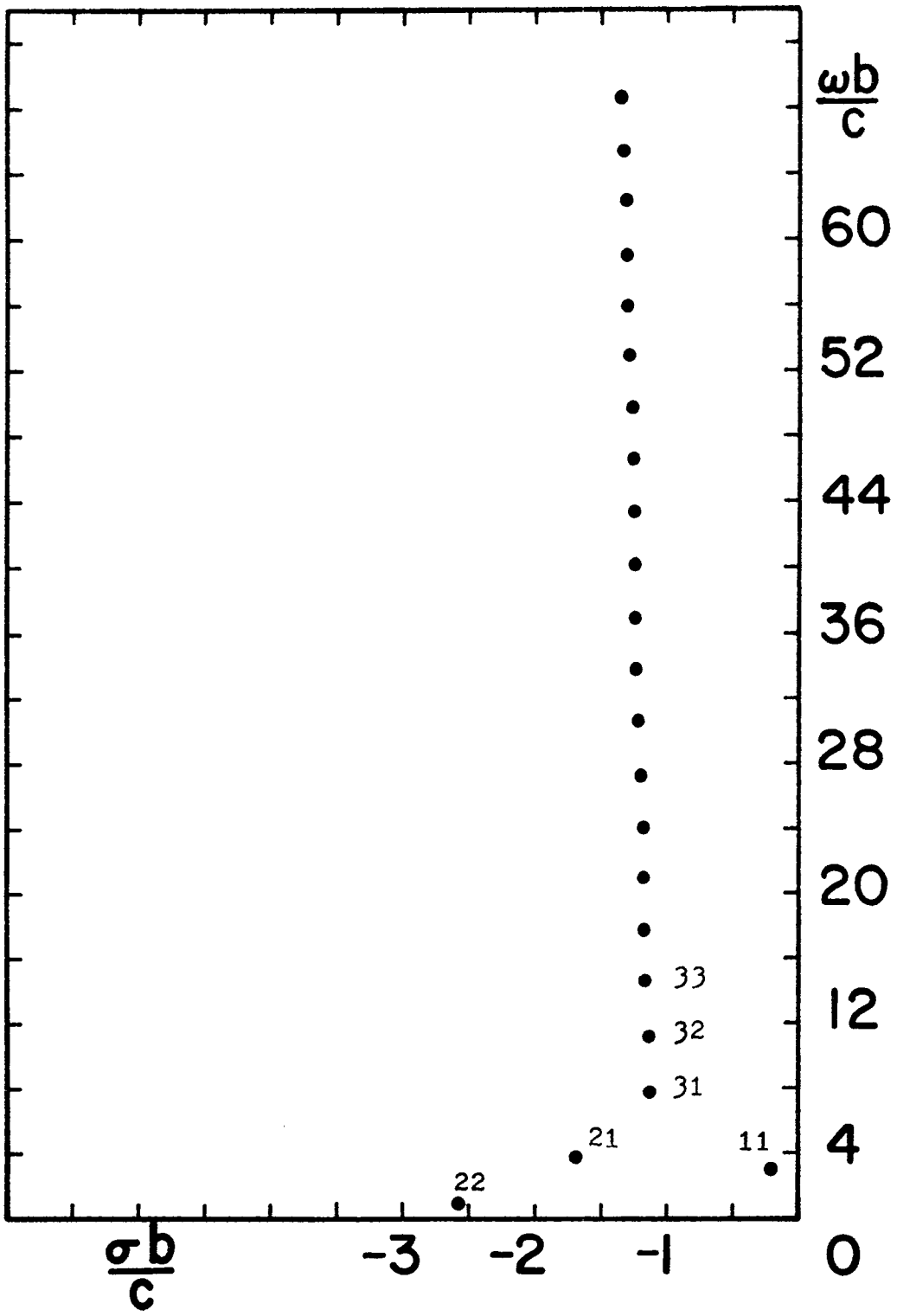

Figure 4 Natural frequencies of circular loop corresponding to third mode (n = 3), Ω = 12.0.

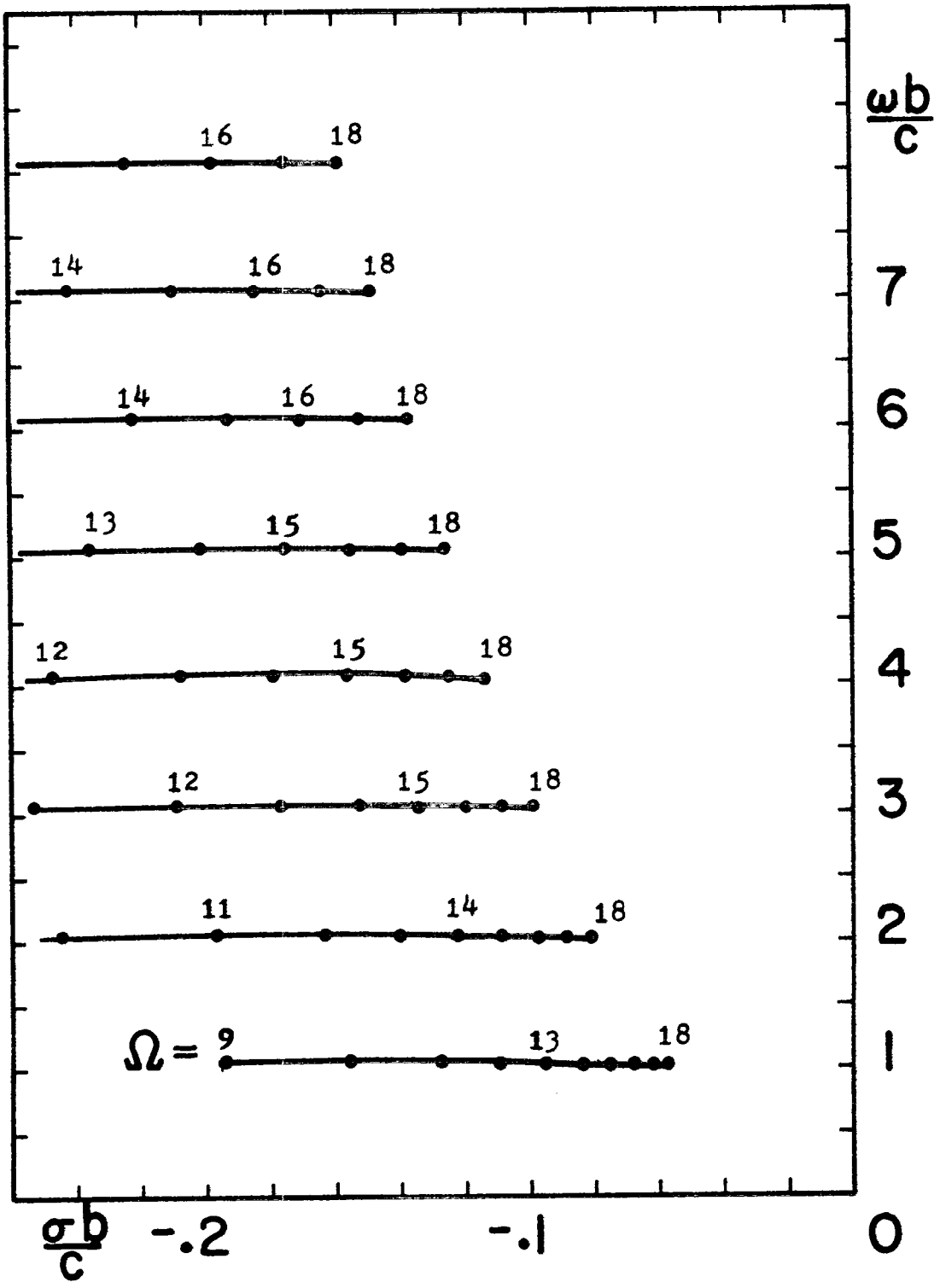

Figure 5 Trajectories of the poles of principal layer $\ell = 1$, as a function of loop parameter Ω.

size Ω. As the loop becomes thicker in cross section the poles move away from the $j\omega$-axis exhibiting increased damping. Figure 6 gives the pole trajectories of the third mode (n = 3) poles as a function of the loop parameter. We note that the pole trajectories corresponding to secondary layers (ℓ = 2) move towards the $j\omega$-axis as the loop becomes thicker in cross section.

Even though asymptotically there exists only two sets of poles of the ℓ = 3 type corresponding to even and odd Fourier modes, at lower frequencies the poles are distinct as shown in Figure 7 corresponding to loop size Ω = 12.0 for modes n = 0 to n = 10.

Figure 8 gives the real and imaginary parts of the residues of the poles in the primary layer ℓ = 1 closest to the $j\omega$-axis as a function of loop parameter Ω for various Fourier modes. The residues monotonically increase for increasing wire radii. The residues of the poles in secondary layers ℓ = 2 are similarly shown in Figures 9-11 . The residues of poles in layers far away from the principal layer lie almost in straight lines as a function of loop size and mode number. Figure 12 gives the residues of a few of the poles of the third layer ℓ = 3.

Using the poles and the residues, the various Fourier coefficients $1/a_n(s)$ can be readily constructed in partial fraction form for time harmonic input excitation and Figures 13a,b show the real and imaginary parts of $1/a_n(j\omega)$ for the first three modes as a function of frequency. The real part of $1/a_n(j\omega)$ is in very good agreement with those obtained by Wu [1] using equation (12) directly for the various Fourier coefficients at every real frequency. But the imaginary parts of $1/a_n(j\omega)$

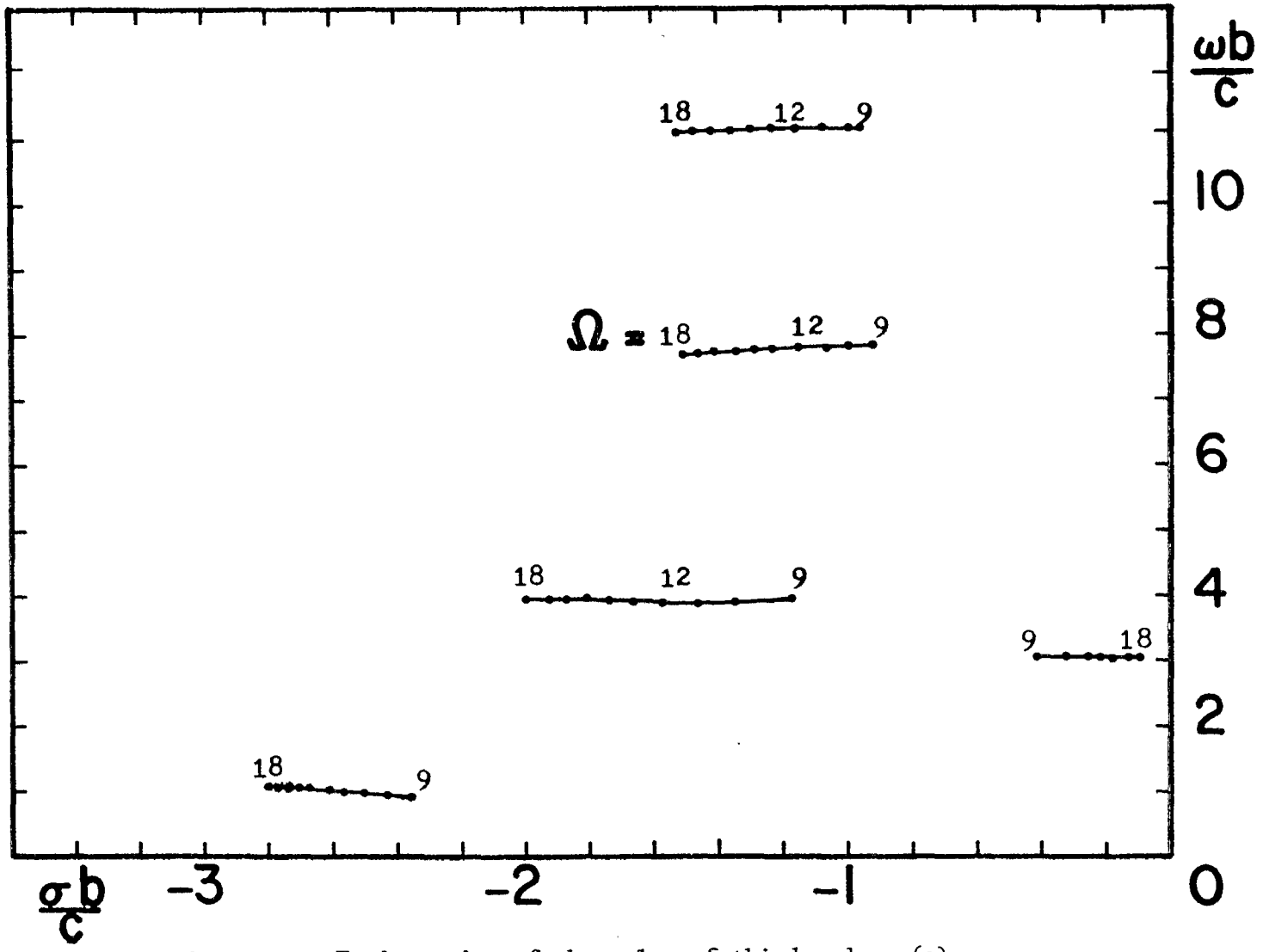

Figure 6 Trajectories of the poles of third mode $a_3(s)$ as a function of loop parameter Ω.

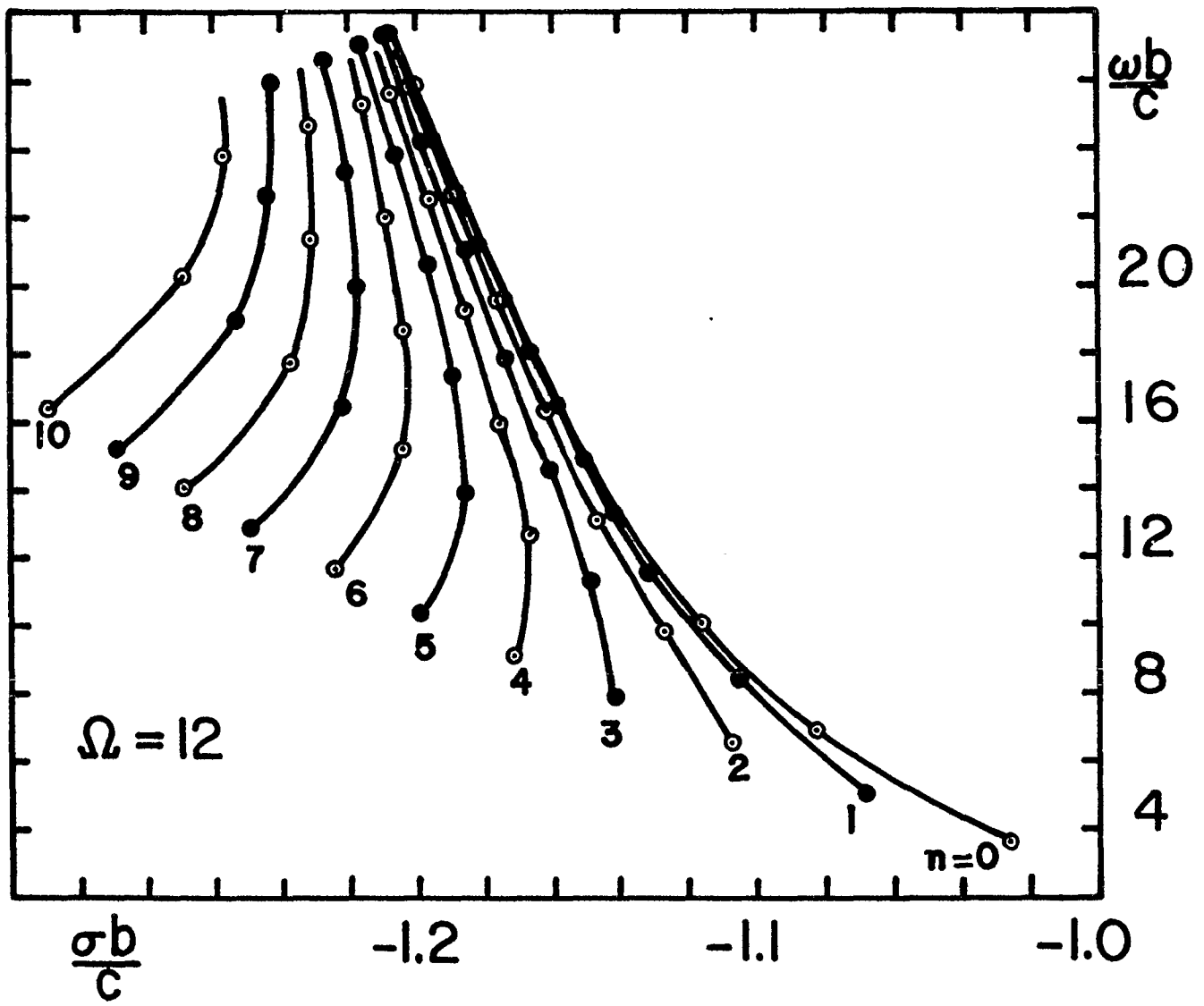

Figure 7 Natural frequencies of circular loop in layer ℓ = 3.

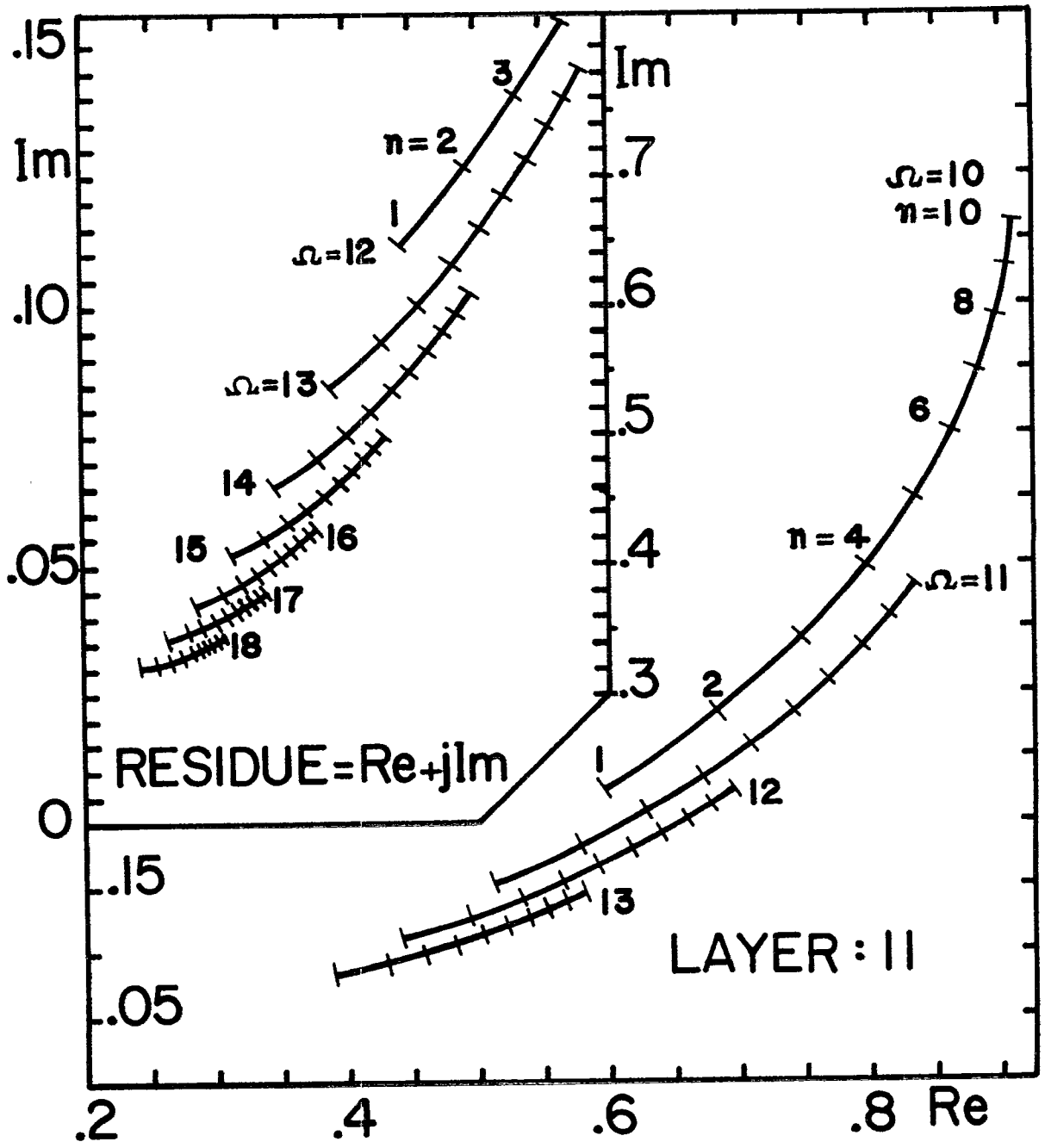

Figure 8 Residues of the poles in principal layer 11 as a function of loop parameter Ω.

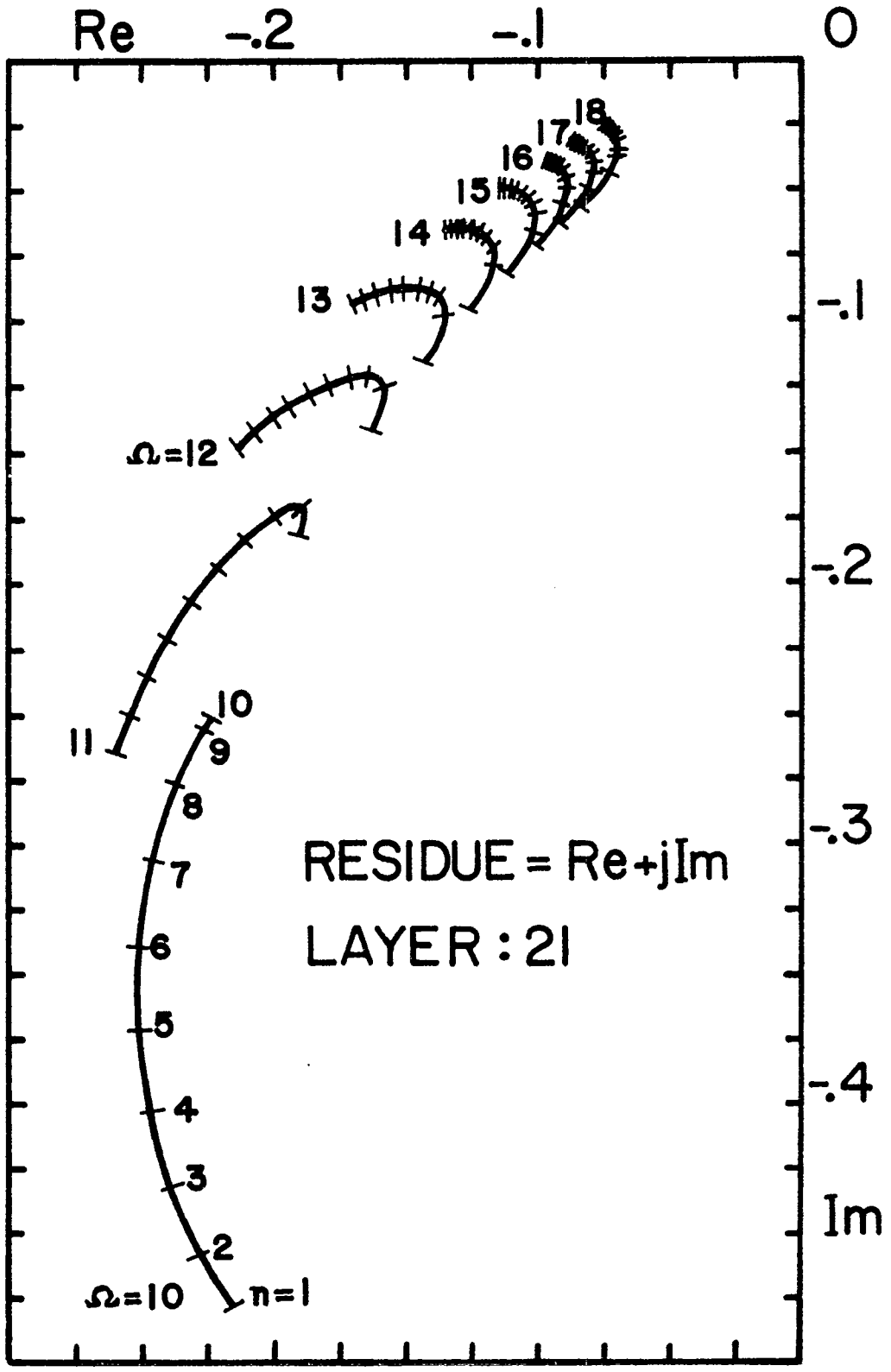

Figure 9 Residues of the poles in secondary layer 21 as a function of loop parameter Ω.

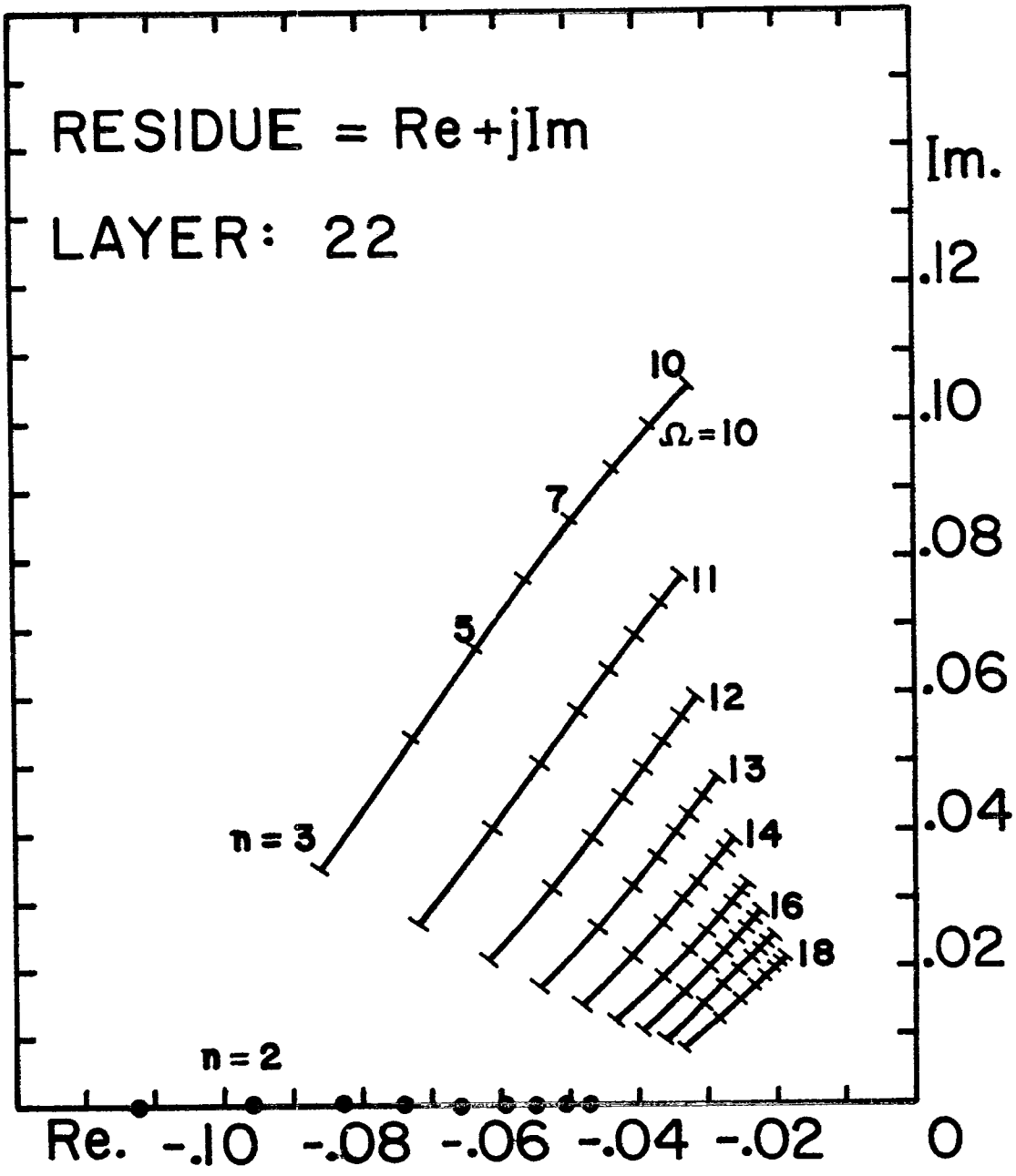

Figure 10 Residues of the poles in secondary layer 22 as a function of loop parameter Ω.

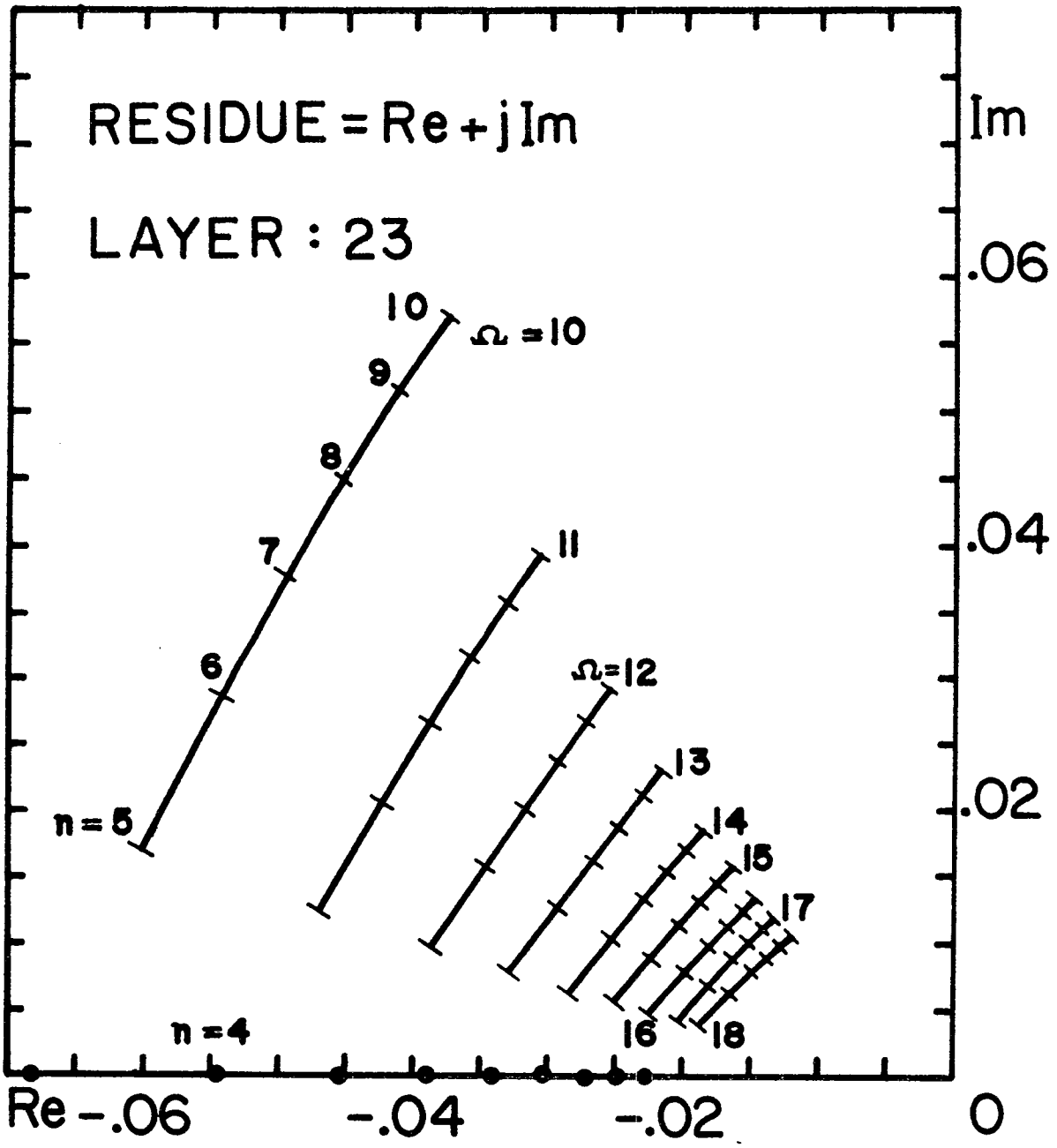

Figure 11 Residues of the poles in secondary layer 23 as a function of loop parameter Ω.

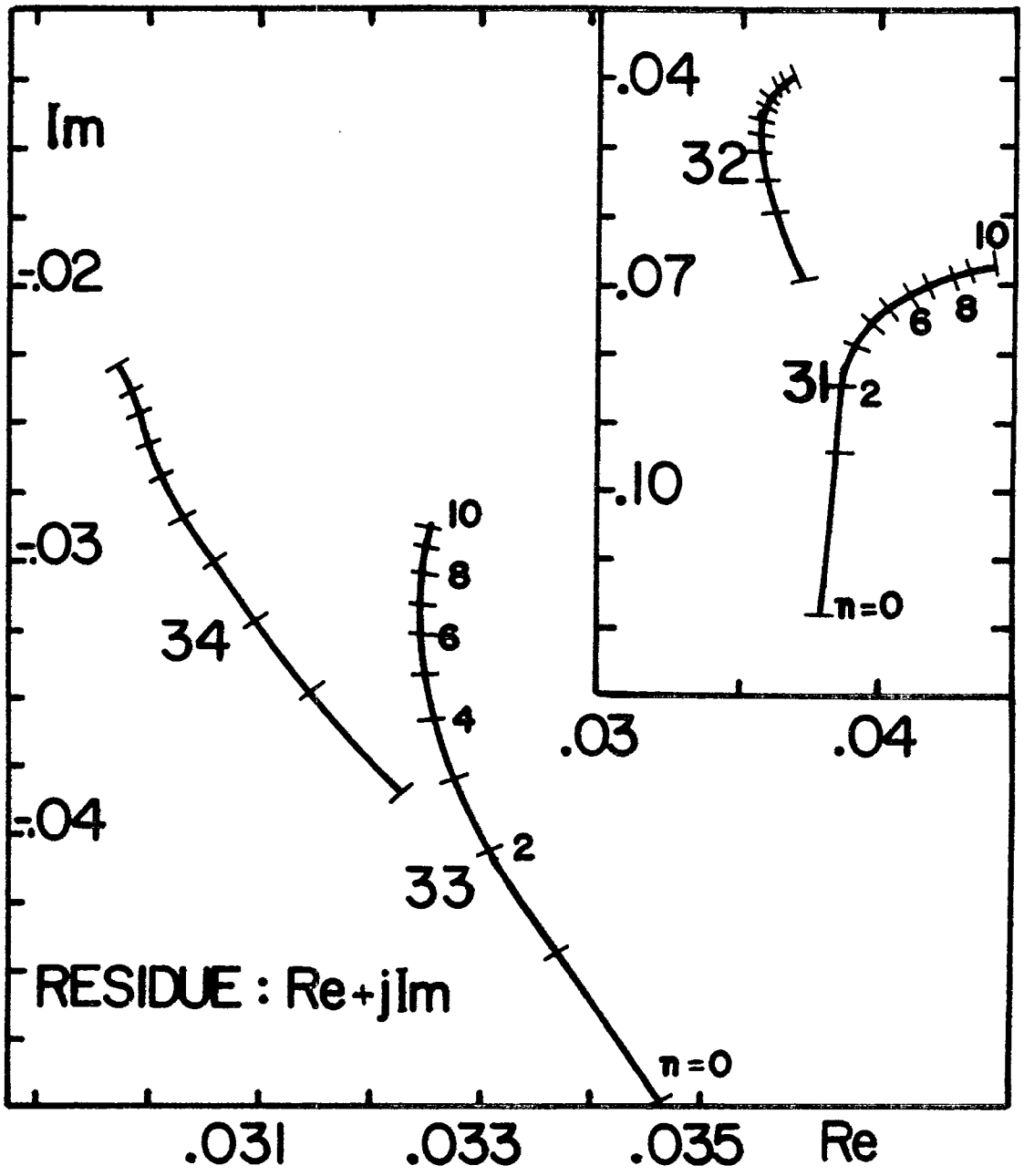

Figure 12 Residues of the poles in third layer ($\ell = 3$), $\Omega = 12.0$.

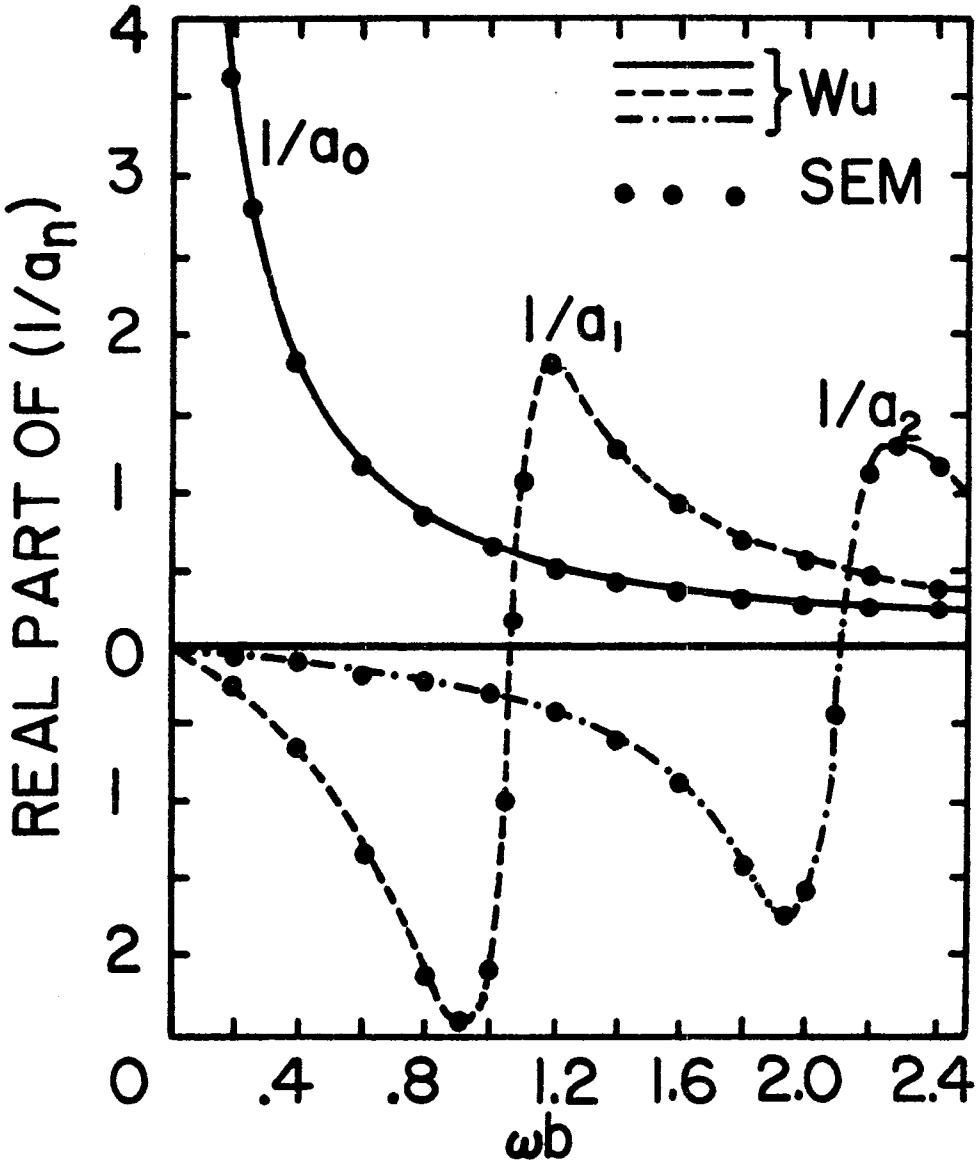

Figure 13a Real part of $1/a_0(s)$, $1/a_1(s)$ and $1/a_2(s)$ as a function of real frequency ω.

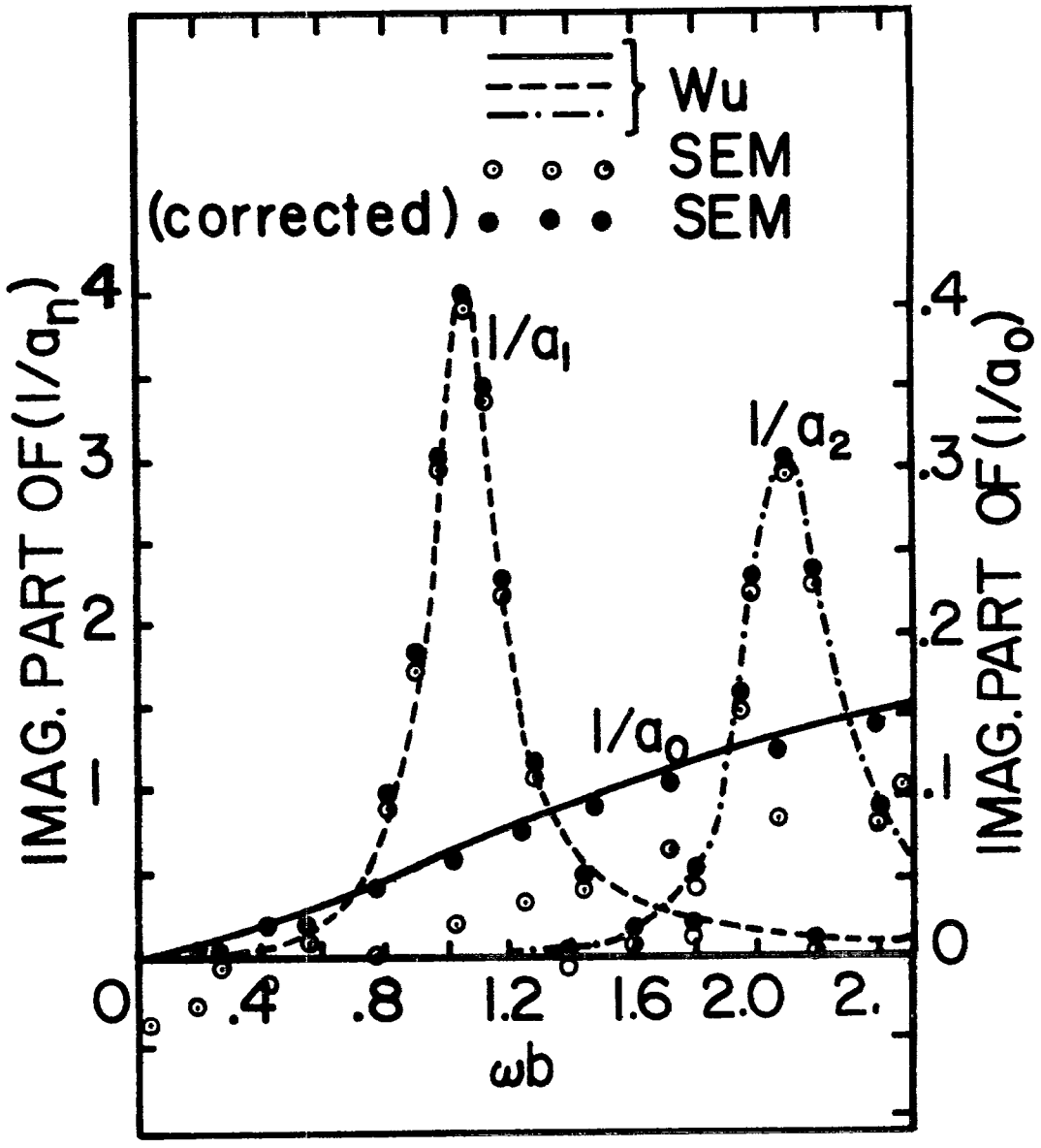

Figure 13b Imaginary part of $1/a_0(s)$, $1/a_1(s)$ and $1/a_2(s)$ as a function of real frequency ω.

obtained by SEM are not in good agreement with those obtained by direct calculations, but appear to differ by a single constant at all frequencies for each of the Fourier modes. Since it is known a priori that these curves should approach zero as s tends to zero, this constant may be found by evaluating the partial fraction at s = 0 and subtracting the resulting constant from all subsequent calculations. While much effort has been expended in attempting to resolve the reason for the constant error, the following explanation is considered the most likely.

We note that according to the residue series expansion (equation 25),

$$\frac{-j}{a_n(s)} = \sum_i \frac{R_{ni}}{s-s_{ni}}$$

where the summation i is over an infinite number of terms including the conjugate pole locations. While calculating $1/a_n(s)$, the series expansion must be truncated in the summation over the infinite number of poles in the $\ell = 3$ layer. At $s = j\omega = 0$

$$\frac{-j}{a_n(0)} = \sum_i \frac{R_{ni}}{-s_{ni}}$$

and this infinite summation should sum to zero if all the poles and the residues have been accurately calculated. The poles and the residues were calculated accurate up to eight decimal places for poles such that $\omega b/c \leq 30$ but the poles and residues far out in the layer

ℓ = 3 were calculated using asymptotic formulas (equations 41A and 48A) developed in Appendix A. The poles and residues calculated by the asymptotic formula differ only in the second decimal place for $\omega b/c < 30$ and yet a summation over a number of them with a small error can introduce a significant constant error in the imaginary parts at all frequencies. This error should then be subtracted out in the numerical processing. It was further verified numerically that the error at s = 0 gradually goes to zero for thin loop structures $\Omega \to 18$ and becomes somewhat large for very large sizes of the loop $\Omega < 10$. This is in apparent agreement with the fact that the asymptotic formula for poles and residues is more accurate for thin loops.

The input admittance of the circular loop antenna (Figures 21-22) excited by a delta gap are given in a later section along with the results obtained for the case of dissipative medium. There, the conductance part of the input admittance is shown corrected because of the term -j appearing in the series which causes the imaginary part of the Fourier coefficients to be reflected in the conductance. Further we note the input susceptance is in very good agreement with the results [2].

Figure 14 shows the time domain current on the circular loop antenna corresponding to a unit delta function in time excitation at the input gap terminals turn on at t = 0. It is a difficult process to construct a delta function with a set of Fourier modes. The first peak shown in the figure gets larger while its width becomes narrower as the number of poles corresponding to modes close to $j\omega$-axis are gradually increased. This time domain plot is constructed by including all the

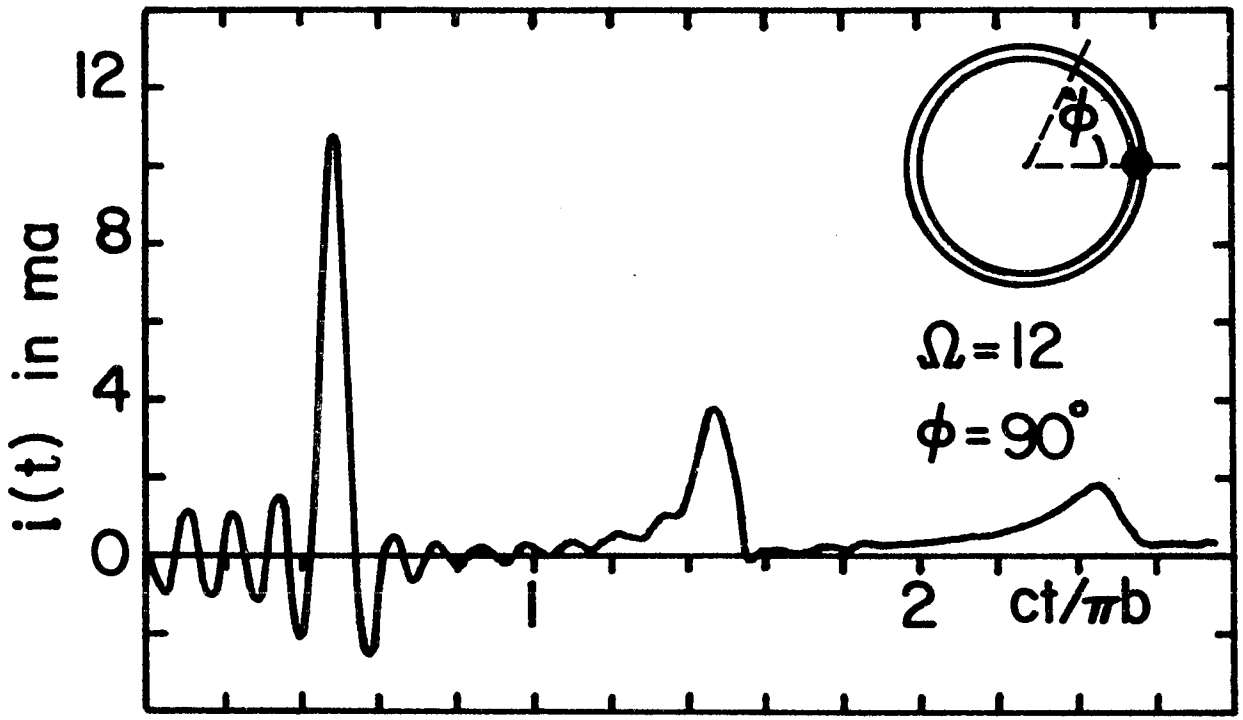

Figure 14 Time domain current observed at $\phi = 90°$ for delta function in time excited at the delta gap at $t = 0$ and $\phi = 0$.

poles and their conjugates given in Figure 3 . We further note the time delay of $ct/\pi b = 0.5$ corresponding to the observation point at $\phi = 90°$. The oscillations before the wave reaches the observation point corresponds to the principal resonance $\ell = 1$ of the highest mode included in constructing the current response, and the oscillations become smaller and smaller as the number of modes are increased.

The time domain current on the circular loop antenna for a finite length unit pulse function in time (constructed by the superposition of two unit step functions) exciting the gap at $t = 0$ is shown in Figure 15. Instead of observing the current response at a single point, the response is shown observed at constant time intervals all along the loop structure. The pulse width is $T = 0.5$ where $T = 1.0$ corresponds to the time necessary to travel half way around the loop at the speed of light. In the current response at time $T = 1.2$, the two pulses traveling in opposite directions around the loop have summed to approximately double the current magnitude.

4. Application of SEM to the circular loop scatterer in free space

The induced current distribution on the circular loop scatterer, Figure 1 , corresponding to a plane wave excitation is obtained by equation (9) and (21) with $\gamma = s/c$ and $\xi = \eta$ the impedance of free space

$$I(\phi,s) = \frac{-j2b}{\eta} E_0^i(s) \sum_{n=-\infty}^{+\infty} \frac{f_n(s)\, e^{-jn\phi}}{a_n(s)} \qquad (31)$$

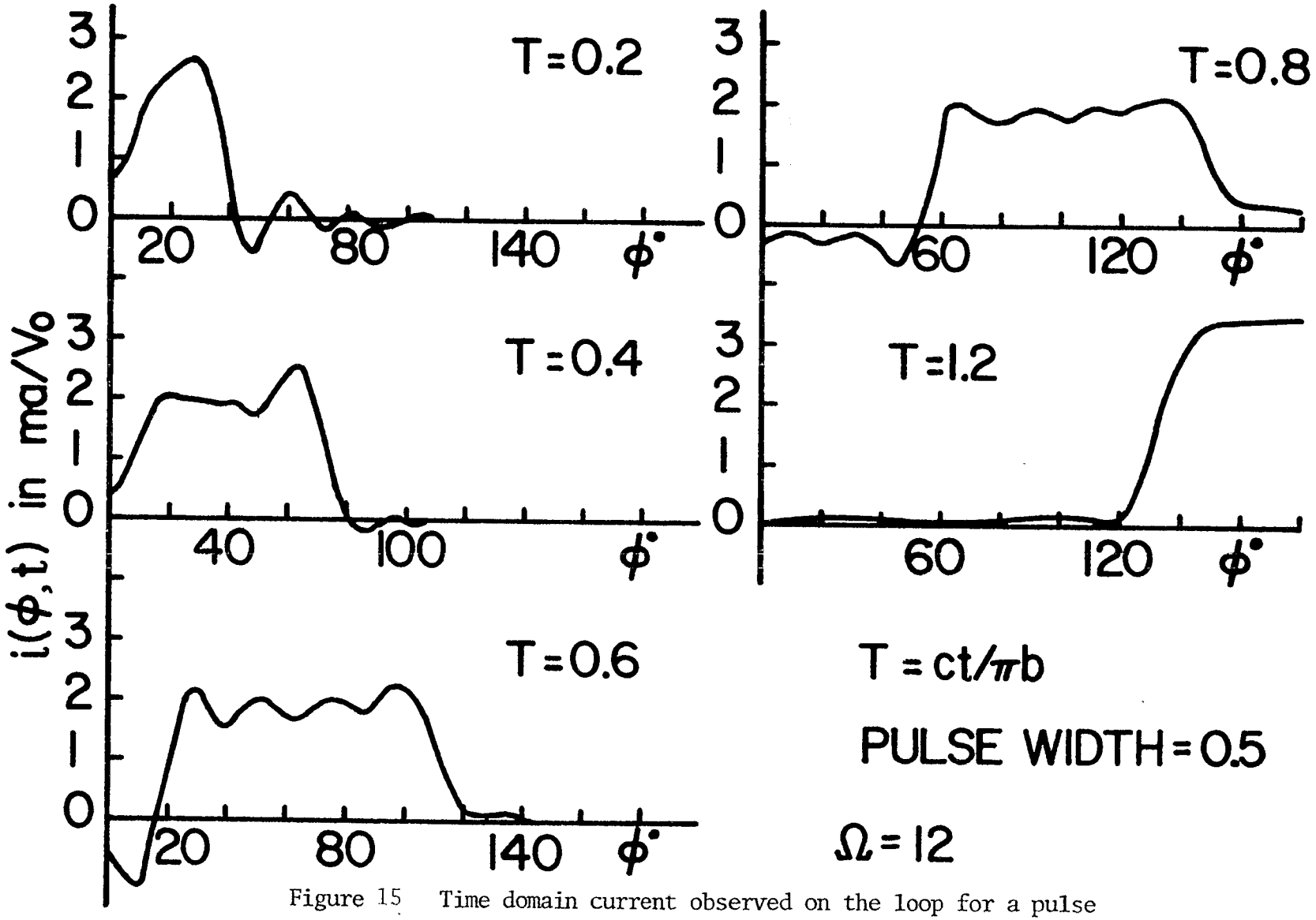

Figure 15 Time domain current observed on the loop for a pulse function in time excited at the delta gap at t = 0 and $\phi = 0$.

We note in the equation (31) the specific advantage of expanding the incident field in a Fourier series in ϕ (equations (16) and (21), i.e., the nth harmonic component of the plane wave excitation couples with only nth component of the current Fourier coefficients. Replacing $1/a_n(s)$ by the residue series (24), the equation 31 becomes

$$I(\phi,s) = \frac{2b}{\eta} E_0^i(s) \sum_{n=-\infty}^{+\infty} \sum_i \frac{R_{ni} e^{-jn\phi}}{s-s_{ni}} f_n(s) \qquad (32)$$

It is now relatively straightforward to obtain the frequency domain solution corresponding to a time harmonic plane wave incident by substituting $s = j\omega$ in the equation (32). To obtain time domain current for plane wave scattering, the Laplace inverse of the equation (32) must be taken,

$$i(\phi,t) = \frac{1}{2\pi j} \int_{C_B} \left[\frac{2b}{\eta} E_0^i(s) \sum_{n=-\infty}^{+\infty} \sum_i \frac{R_{ni} e^{-jn\phi}}{s-s_{ni}} f_n(s)\right] e^{st}\, ds \qquad (33)$$

where $f_n(s)$ are the nth coefficient of the incident plane wave excitation defined in the equation (21).

Depending on the incident angles, the coefficients (from equation (21),

$$f_n(s) = \begin{cases} J_n'(-j\frac{\alpha sb}{c})\, j^{n-1} \cos\psi\, e^{-jn\phi_0} \\ \quad \text{and/or} \\ \dfrac{J_n(-j\frac{\alpha sb}{c})}{-j\frac{\alpha sb}{c}}\, j^n \sin\psi \cos\theta\, e^{-jn\phi_0} \end{cases}$$

To Laplace invert the equation (33) term by term, the asymptotic behavior of $f_n(s)$ is required. If $\alpha = \sin\theta$ is the direction cosine of the incident field with respect to the plane of the loop, the time domain Fourier components of the current

$$i_n(t) = \frac{1}{2\pi j}\int_{C_B} \frac{2b}{\eta}\left[\sum_i \frac{R_{ni}}{s-s_{ni}} f_n(s)\right] e^{st}\, ds \tag{34}$$

and asymptotically $f_n(s)$ [3] can be written as

$$f_n(s) \xrightarrow[s\to\infty]{} \begin{cases} \sqrt{2jc/\pi\alpha sb}\,\cosh\left[\frac{\alpha sb}{c} + j\frac{\pi}{4} + j(n-1)\frac{\pi}{2}\right] \\ \sqrt{2j/\pi}\left[\frac{\alpha sb}{c}\right]^{-3/2}\cosh\left[\frac{\alpha sb}{c} + j\frac{\pi}{4} + jn\frac{\pi}{2}\right] \end{cases} \tag{35}$$

Since

$$e^{st}\cosh\frac{\alpha sb}{c} \sim \begin{cases} e^{+\frac{\alpha sb}{c} + st}, & \text{as } s\to\infty \text{ in R.H.P.} \\ e^{-\frac{\alpha sb}{c} + st}, & \text{as } s\to\infty \text{ in L.H.P.} \end{cases} \tag{36}$$

The contour may not be closed for $|t|<\alpha b/c$ in either half-plane, Figure 16c. There are at least three alternative methods to resolve this difficulty, all resulting in different representations.

METHOD I

We shall express the term $J_n(-j\frac{\alpha sb}{c})$ in terms of two Hankel functions

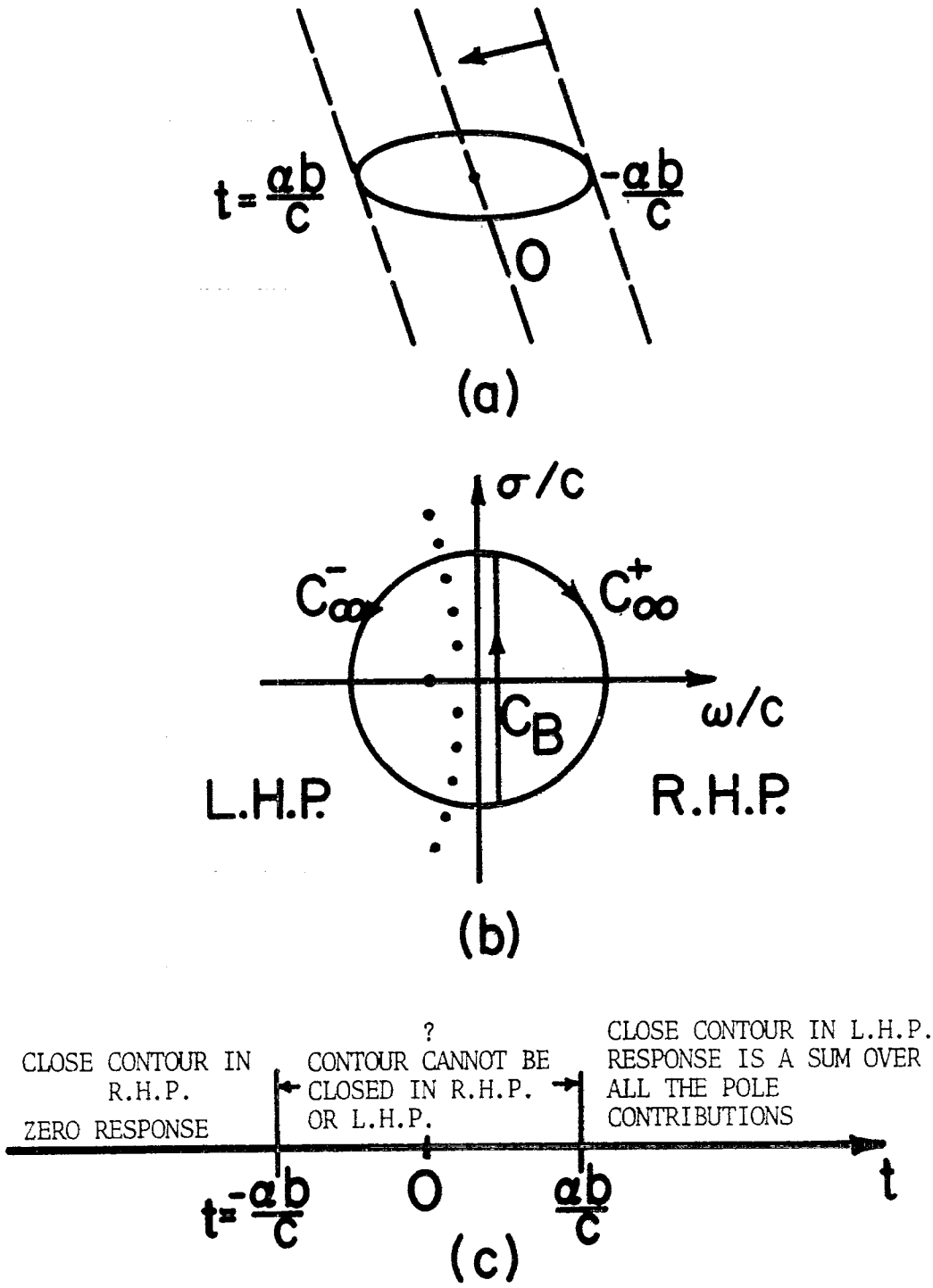

Figure 16. Illustration of contour closure.

$$J_n(-j\frac{\alpha sb}{c}) = H_n^{(1)}(-j\frac{\alpha sb}{c}) + H_n^{(2)}(-j\frac{\alpha sb}{c}) \tag{37}$$

Hence as $s\to\infty$ [3]

$$e^{st} H_n^{(1)}(-j\frac{s\alpha b}{c}) \sim \sqrt{\frac{2c}{\pi\alpha sb}}\, j^{-n} e^{\frac{\alpha sb}{c} + st} \tag{38}$$

and

$$e^{st} H_n^{(2)}(-j\frac{s\alpha b}{c}) \sim \sqrt{\frac{-2c}{\pi\alpha sb}}\, j^{n} e^{-\frac{\alpha sb}{c} + st} \tag{39}$$

For the terms

$$\left\{ \begin{array}{l} H_n^{(1)} \\ H_n^{(2)} \end{array} \right\}$$

we now close the contour C_B in left half plane for (Figure 17b)

$$\left\{ \begin{array}{l} t > -\frac{\alpha b}{c} \\ t > +\frac{\alpha b}{c} \end{array} \right\} \tag{40}$$

Unfortunately, $H_n^{(1)}$ and $H_n^{(2)}$ have branch cuts along the negative real axis as shown in **Figure** 17a, and one has to evaluate the branch cut contributions in addition to the poles contribution for the time interval $|t|<ct/b$.

METHOD II

To get rid of branch cut integral contributions, we note that the

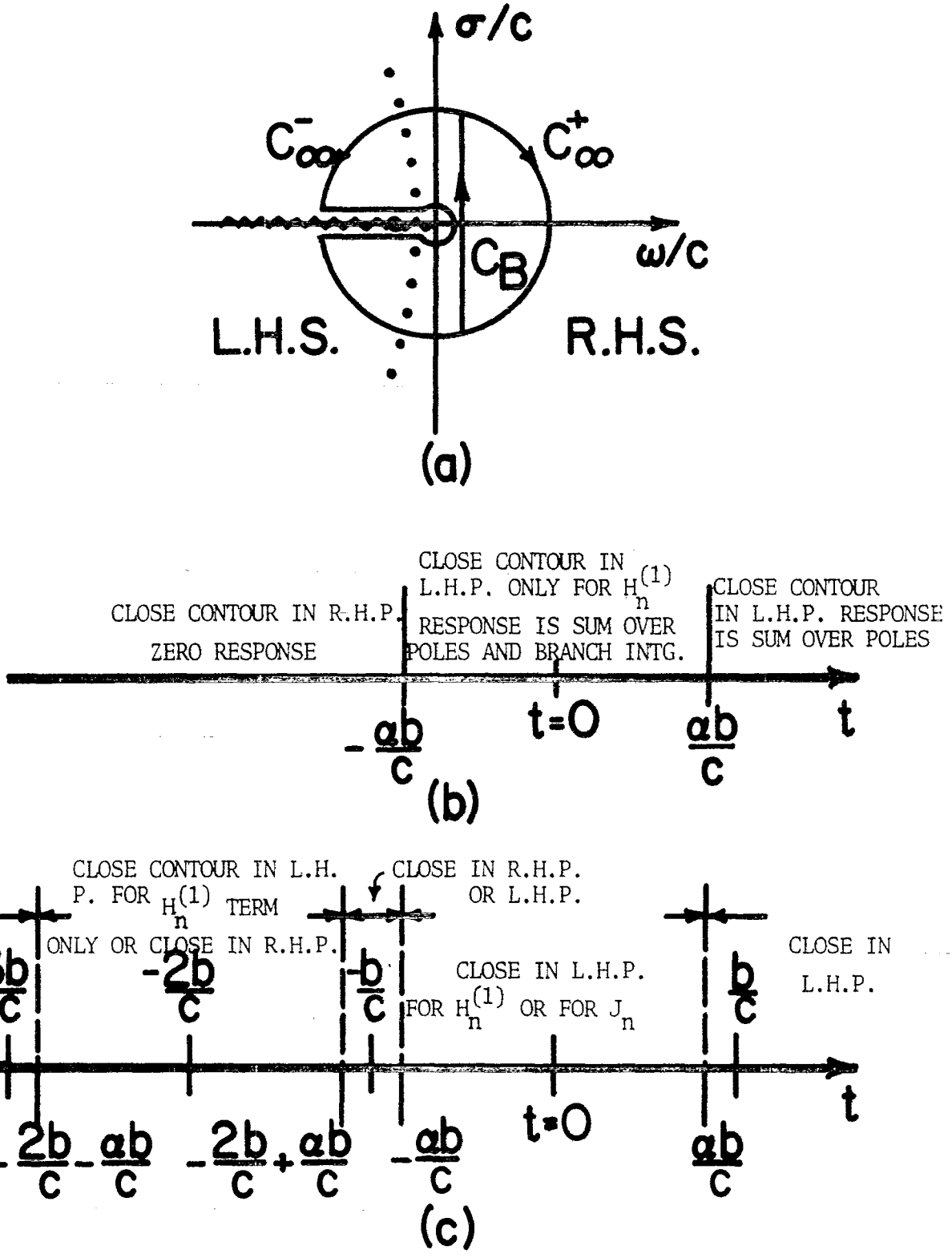

Figure 17. Illustration of contour closure for different intervals.

incident field due to plane wave excitation could just as easily have been expanded in terms of spherical harmonics

$$\hat{J}_n(-j\,\frac{\alpha sb}{c}) = \hat{H}_n^{(1)}(-j\,\frac{\alpha sb}{c}) + \hat{H}_n^{(2)}(-j\,\frac{\alpha sb}{c}) \tag{41}$$

The contour closure is the same as in the previous method, hence [4]

$$e^{st}\,\hat{H}_n^{(1)}(-j\,\frac{\alpha sb}{c}) \sim -j^{-n+1}\,e^{\frac{\alpha sb}{c} + st}$$

$$e^{st}\,\hat{H}_n^{(2)}(-j\,\frac{\alpha sb}{c}) \sim j^{n+1}\,e^{-\frac{\alpha sb}{c} + st} \quad \text{as } s\to\infty \tag{42}$$

and $\hat{H}_n^{(1)}$ has no branch cuts in the complex s plane. We still have, however, the inconvenience of using different representations for the response over certain time intervals. In the following method, this difficulty is alleviated.

METHOD III

Instead of Laplace inverting the series (33) term by term, we consider the asymptotic behavior of $1/a_n(s)$ as a whole in the equation (33). It is shown in the Appendix A, equation 39A,

$$\frac{1}{a_n(s)} \sim \frac{1}{\frac{sb}{c}\left[-2\ell n\,\frac{sb}{c} + (-1)^{n+1}\sqrt{\frac{c\pi}{sb}}\,e^{-\frac{2sb}{c}}\right]}, \quad s\to\infty \tag{43}$$

$$\sim \begin{cases} \dfrac{1}{-\dfrac{sb}{c}\, 2\ell n\, \dfrac{sb}{c}} , & \text{as } s\to\infty \text{ in R.H.P.} \\ \dfrac{1}{(-1)^{n+1}\, \dfrac{sb}{c}\sqrt{\dfrac{c\pi}{sb}}}\, e^{+\frac{2sb}{c}} , & \text{as } s\to\infty \text{ in L.H.P.} \end{cases} \qquad (44)$$

Hence, we could have closed the contour in the left half plane 2b/c seconds earlier than the times stated in the previous two methods as shown in the Figure 17c. Since the incident wave first excites the loop at $t = -\alpha b/c$, the contour C_B can be closed in LHP for all times $t > -\alpha b/c$.

It is interesting to point out that in the time interval $(-2+\alpha)b/c < t < -\alpha b/c$, the contour may be closed in either the right or left half plane. Since the excitation does not begin until $t = -\alpha b/c$, the residue series must sum to zero during this time interval. These examples clearly point out a non-uniqueness feature in the representation of time domain results.

5. Numerical results for circular loop scatterer in free space

The equation (33) for the time domain current on the circular loop scatterer for a step function plane wave excitation is evaluated for incidence angles $\phi_0 = 0°$, $\theta = 30°$ and $\psi = 60°$ (Figure 1). The contour C_B in the complex s plane is closed according to the method III described in Section 4 and the time domain current result observed at $\phi = 90°$ is shown in Figure 18. The incident wave front first

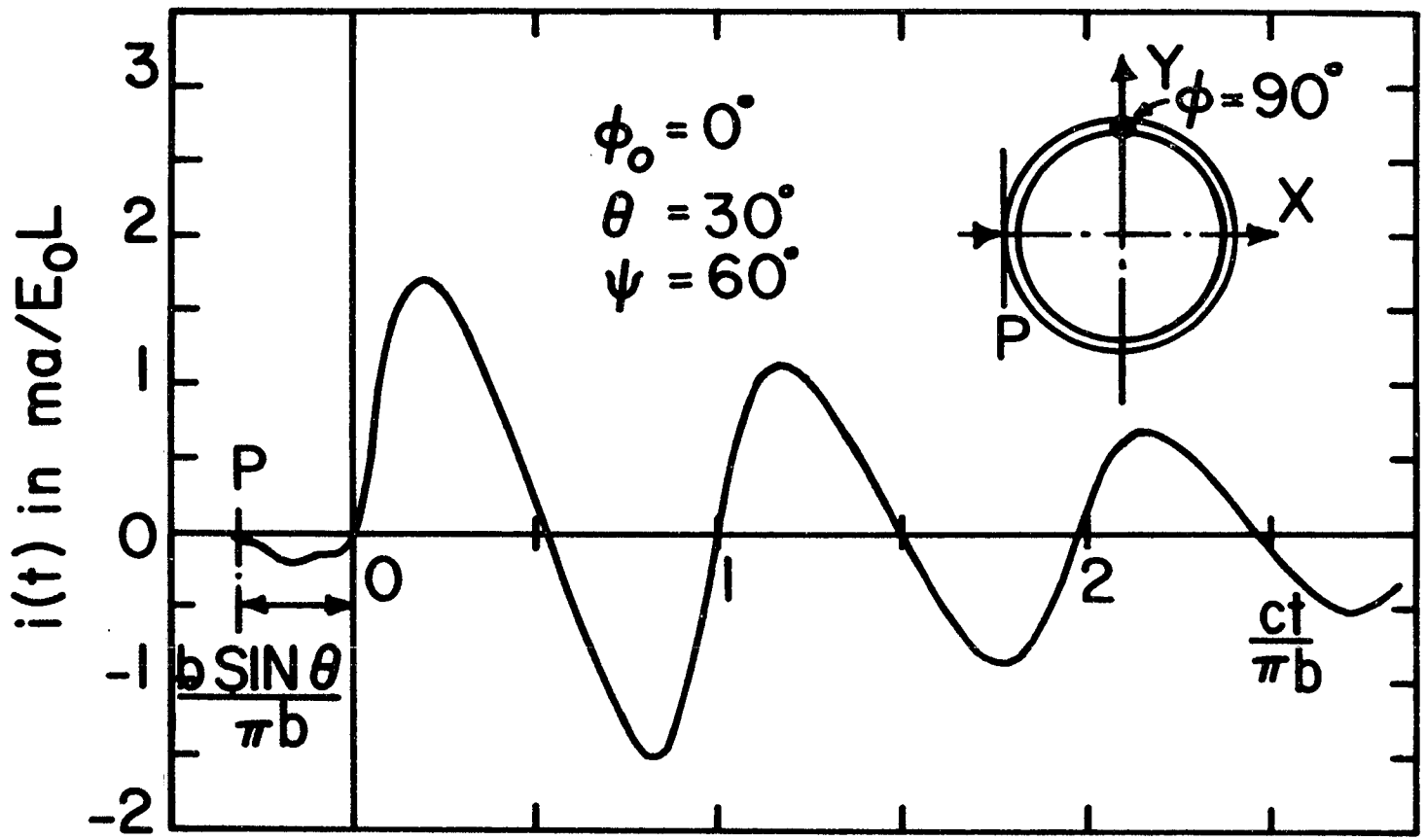

Figure 18. Time domain current, step plane wave incident, $\Omega = 12.0$, $t = 0$ at the origin.

excites the structure at $t = -b \sin\theta/c$ and reaches the center of the loop at $t = 0$. For large values of time, the time domain current gradually decays to zero. Because the observation point is at $\phi = 90°$, there is no contribution from any of the modes with n odd (Equation 31). The response is seen to consist primarily of a contribution from the principal pole ($\ell = 1$) for $n = 2$.

6. Circular loop antenna in dissipative medium and application of SEM

The analysis of the circular loop in lossless free space medium was carried out in previous sections and using SEM we were able to characterize the structure as to its transient scattering behavior. The analysis can be simply extended to the situation wherein the medium is dissipative. We demonstrate in the following how conveniently one can characterize the loop antenna structure in a dissipative medium without re-solving the problem again, i.e., the frequency and the time domain results can be obtained by making use of the resonant frequencies and the corresponding residues obtained for the lossless free space medium. While this method can be used for any perfectly conducting object, it is particularly simple to illustrate for the loop.

The current distribution on the circular loop antenna is given by equations (9) and (19)

$$I(\phi,s) = \sum_{n=-\infty}^{+\infty} I_n(s)e^{-jn\phi} \qquad (45)$$

and

$$I_n(s) = \frac{-jV_0(s)}{\xi\pi} \frac{1}{a_n[\gamma(s)]} \tag{46}$$

In equation (46), we write the Fourier coefficient a_n as a function of $\gamma(s)$, where γ is the complex propagation constant of the medium given by

$$\gamma = \alpha + j\beta = [\mu s(\varepsilon s + \sigma_c)]^{\frac{1}{2}} \tag{47}$$

where σ_c is the conductivity of the medium assumed to be independent of s, and again μ and ε are the (frequency independent) permeability and the permittivity of the medium.

For the lossless free space medium $\sigma_c = 0$ and therefore, $\gamma = s/c$. In the equation (46), the term

$$\frac{1}{\xi} = \frac{1}{\eta} \frac{\sqrt{\frac{s}{c}(\frac{s}{c} + A)}}{\frac{s}{c}} \tag{48}$$

where $\eta = \sqrt{\mu/\varepsilon}$ is the impedance of the lossless medium with parameters μ and ε. We have also introduced the normalized conductivity of the medium

$$A = \frac{\sigma_c}{\varepsilon c} \tag{49}$$

The residue series developed in Appendix A, equation (56A) can be substituted into (46) with the s/c variable in the equation (56A) replaced by γ which amounts to stating that the poles and the residues

already determined for the lossless free space case correspond to the γ plane. We note referring to equation (48), that the s plane has a branch cut singularity on the negative real axis, Figure 19, between the two branch points s/c = 0 and s/c = -A. If $\gamma = \gamma_{ni}$ are the pole locations in the γ plane for $1/a_n(\gamma)$ for the lossless case (A = 0), these poles are shifted to new locations for a given A in the s plane, which may be found as the solution to the quadratic equation

$$\left[\frac{s_{ni}}{c}\right]^2 + A\left[\frac{s_{ni}}{c}\right] - \gamma_{ni}^2 = 0 \tag{50}$$

where the appropriate choice of the root must be taken.

Hence in the γ plane, by equations (45), (46), (47), and (48), the Laplace current transformed current distribution on the circular loop antenna excited by a delta gap at $\phi = 0$, is given by

$$I(\phi,\gamma) = \frac{V_0(s)}{\xi\pi} \sum_n \sum_i \frac{R_{ni}/c}{\gamma-\gamma_{ni}} e^{-jn\phi} \tag{51}$$

By substituting $s = j\omega$, the current distribution on the loop can be calculated in the frequency domain corresponding to time harmonic input excitation. The normalized input admittance at the delta gap terminals is obtained by substituting $\phi = 0$, $V_0(s) = V_0$, in equation (51) and rearranging the terms (Figure 20)

$$\frac{Y}{\Delta} = \frac{V_0}{\eta\pi}\left[1 - j\frac{\alpha}{\beta}\right] \sum_n \sum_i \frac{R_{ni}/c}{\gamma-\gamma_{ni}} \tag{52}$$

where [2]

$$\gamma = |\gamma| e^{j\theta} \quad , \quad \theta = \tan^{-1} \frac{\alpha}{\beta} \tag{53}$$

$$\Delta = [\varepsilon_r/\mu_r]^{\frac{1}{2}} \cosh[\tfrac{1}{2} \sinh^{-1} p] \tag{54}$$

ε_r and μ_r are the relative permittivity and the permeability of the medium, and $p = \sigma_c/\omega\varepsilon$ is the loss-tangent.

The time domain current for the circular loop antenna in the dissipative medium is obtained by Laplace inversion of the equation (51) resulting in

$$i(\phi,t) = \sum_{n=-\infty}^{+\infty} i_n(t) e^{-jn\phi} \tag{55}$$

where

$$i_n(t) = \mathcal{L}^{-1} I_n(s) = \int_{C_B} I_n(s) e^{st} \, ds \tag{56}$$

For a step function delayed in time exciting the gap terminals at $\phi = 0$, $t = \tau$ then

$$V_0(s) = V_0 \frac{e^{-s\tau}}{s} \tag{57}$$

and substituting into equation (56) , yields

$$i_n(t) = \frac{1}{2\pi j} \int_{C_B} \frac{V_0}{\eta\pi} \left[\sum_i \frac{R_{ni}/c}{\sqrt{\frac{s}{c}(\frac{s}{c} + A)} - \gamma_{ni}} \right] \frac{\sqrt{\frac{s}{c}(\frac{s}{c} + A)}}{(\frac{s}{c})^2} e^{\frac{s}{c}[ct - c\tau]} \frac{ds}{c} \tag{58}$$

We note that all the singularities including the branch line are to the left of C_B in the left half plane so that for $ct < c\tau$, the contour C_B is closed in right half plane and $i_n(t)$ is zero. For $ct > c\tau$, the contour C_B is closed in the left half plane as shown in the Figure 19, so that the branch line is never crossed. We further note while closing the contour C_B,

(i) the pole of $1/a_0$ at the origin in the γ plane shifts to a pole at the branch point $s/c = -A$

(ii) no poles exist for any mode in between the branch points

(iii) there is a double pole at the origin

(iv) poles on the negative real axis in the γ plane shift to poles on the negative real axis in the s plane, but away from branch point $s/c = -A$.

Hence according to the residue theorem, the time domain current

$$i_n(t) = i_{n1}(t) + i_{n2}(t) + i_{n3}(t) + i_{n4}(t) \tag{59}$$

where

$$i_{n1}(t) = \text{contribution due to the shifted simple poles including their conjugates}$$

$$= \frac{V_0}{n\pi} \sum_i R'_{ni}\, u[ct - c\tau] e^{\frac{s_{ni}}{c}[ct - c\tau]} \tag{60}$$

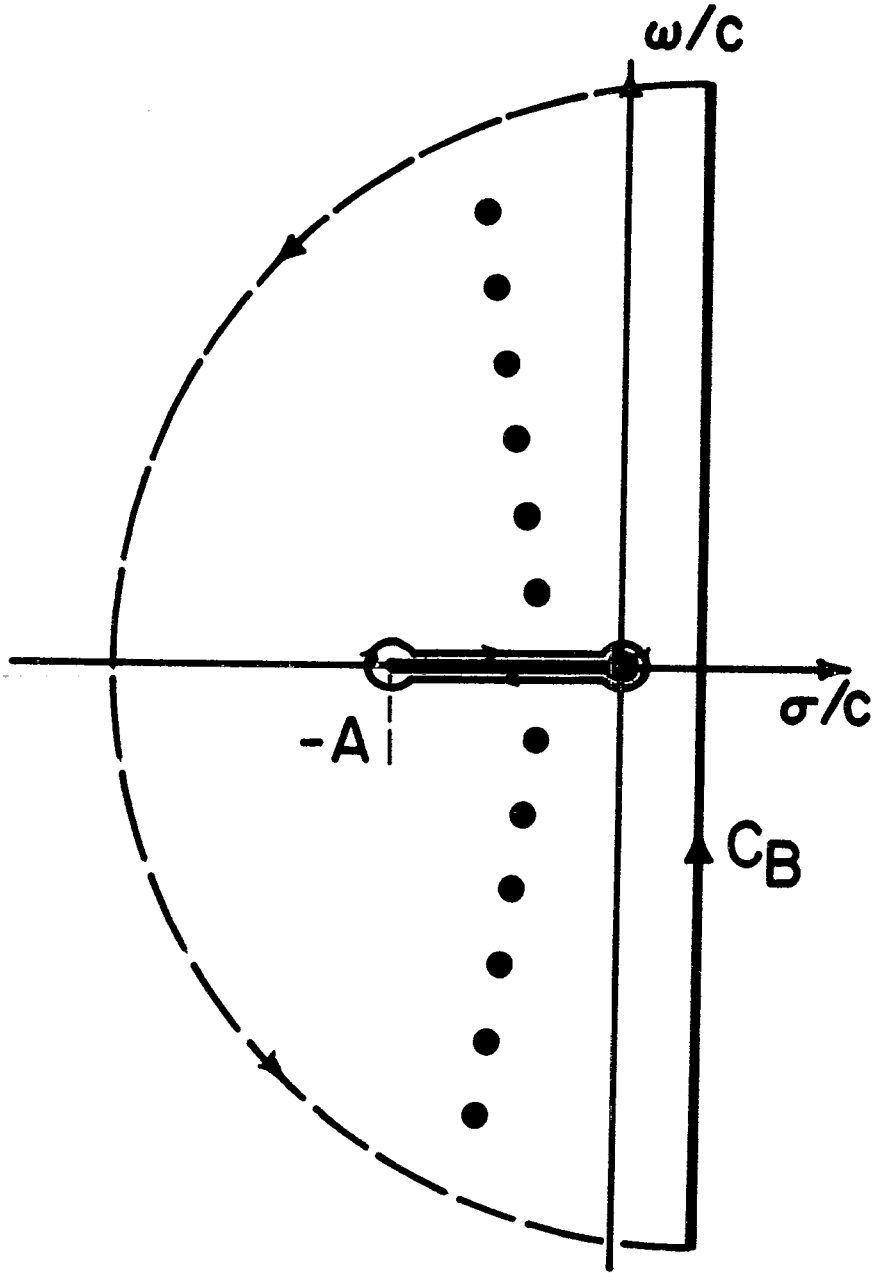

Figure 19. Branch cut in s-plane.

and $s = s_{ni}$ are the zeros of the equation (50) and R'_{ni} are the new residues at $s = s_{ni}$ given by

$$R'_{ni} = \left[\frac{\left[\frac{s}{c} - \frac{s_{ni}}{c}\right]\left[R_{ni}/c\right]\sqrt{\frac{s}{c}\left(\frac{s}{c} + A\right)}}{\left[\sqrt{\frac{s}{c}\left(\frac{s}{c} + A\right)} - \gamma_{ni}\right]\left(\frac{s}{c}\right)^2} \right]_{\frac{s}{c} \to \frac{s_{ni}}{c}} \tag{61}$$

$i_{n2}(t)$ = branch cut contribution obtained by integrating along CD and FG

$$= \frac{V_0}{n\pi^2} \int_0^A \left[\sum_i \frac{-\gamma_{ni} R_{ni}/c}{\sigma(A-\sigma) + \gamma_{ni}^2} \right] \frac{\sqrt{\sigma(A-\sigma)}}{\sigma^2} e^{-\sigma[ct - c\tau]} d\sigma \tag{62}$$

which can be conveniently evaluated numerically. The integrand has a smooth variation and is zero at both the limits of integration

$i_{n3}(t)$ = contribution due to the integration GIC around the branch point $s/c = -A$

$= 0$ for all n (63)

and

$i_{n4}(t)$ = contribution due to the integration DEF around the branch point $s/c = 0$

$= 0$ since we must have $\sum_i \frac{R_{ni}/c}{\gamma_{ni}} = 0$, $n \neq 0$.

But when $\gamma_{ni} = 0$ (pole at the origin in the γ plane due to $1/a_0$)

$$i_{n4}(t) = \frac{V_0}{n\pi}[R_{00}/c][ct - c\tau]u[ct - c\tau],\ n = 0 \qquad (64)$$

Hence the time domain current in the dissipative medium is given by substituting (59) into the equation (55).

7. Numerical results for circular loop antenna in dissipative medium

The input admittance of the loop antenna placed in dissipative medium for time harmonic excitation at the delta gap terminals are presented in this section. Also given are the time domain currents for the loop antenna in a lossy medium for finite width pulse excitation (as a superposition of two step functions displaced in time).

Figure 21 gives the input conductance of the loop antenna as a function of $Im\gamma = \beta$ with the ratio of α/β held constant. The case $\alpha/\beta = 0.0$ corresponds to lossless free space. The computed results by SEM according to equation 52 , have been corrected for the constant error which appeared in the partial fraction expansion (equation 25) at all points in the γ-plane according to the discussion in Section 3. For the lossy cases with $\alpha/\beta = 0.05$ and 0.1 only the corrected SEM results are shown. The correction term is found by summing the series at $\beta=0$ and applied to all the curves in Figure 21. These SEM corrected results are in good agreement with those obtained by King & Harrison [2]. Figure 22 shows the corresponding results for the input susceptance. The above results are computed by SEM making use of all the poles shown in Figure 3 plus as many as 15 poles of the type (iii),

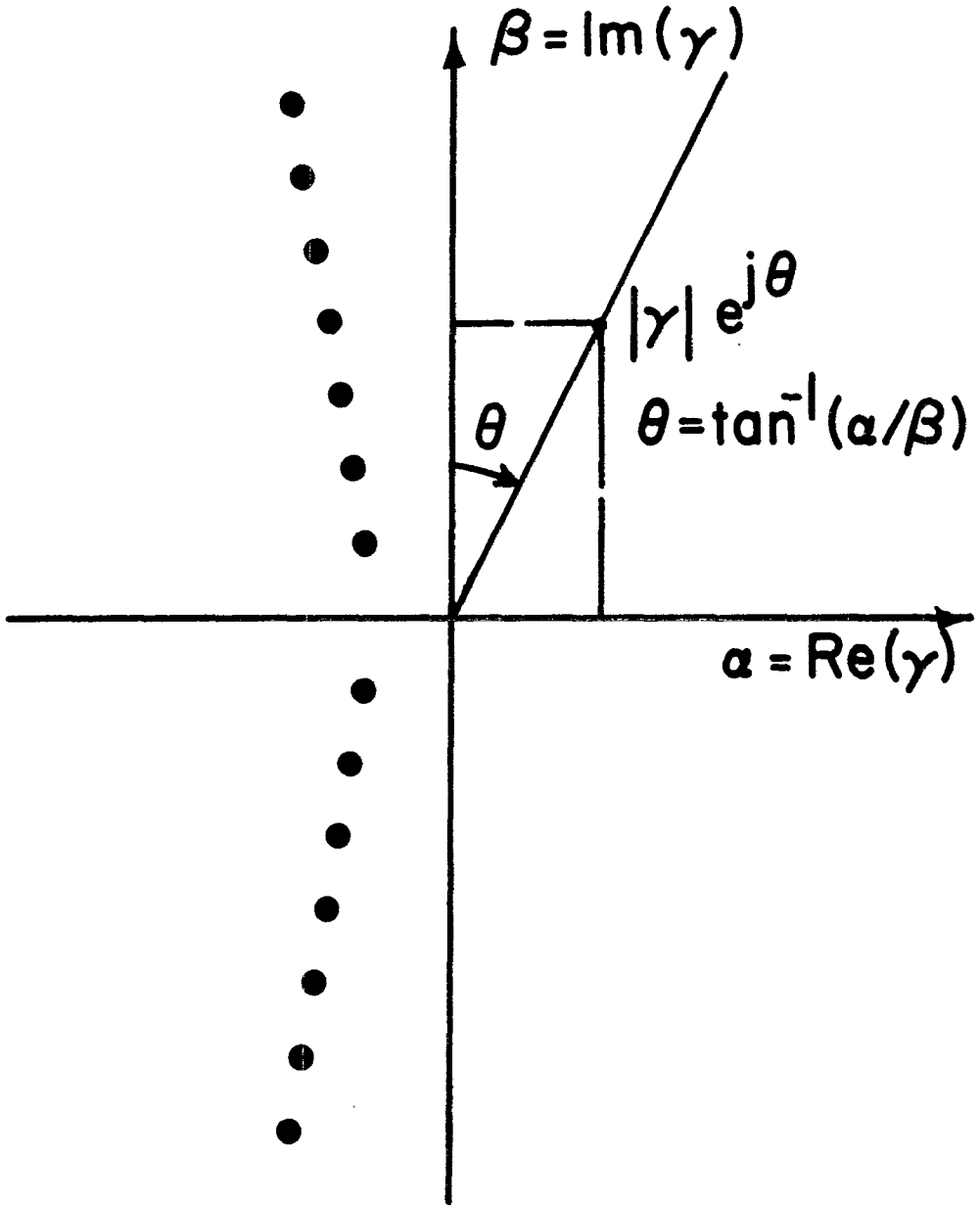

Figure 20 Radial line in γ-plane for a given α/β ratio.

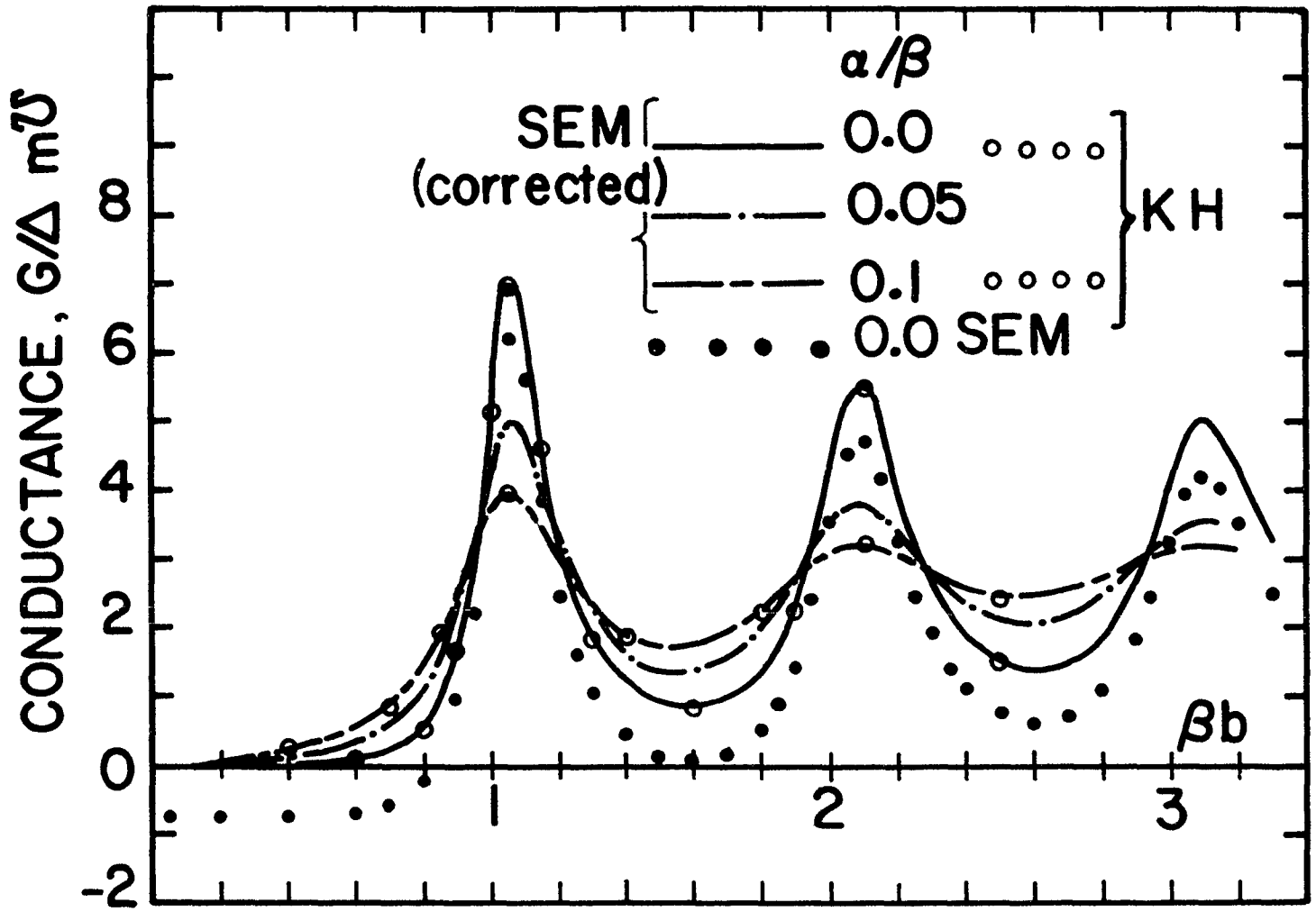

Figure 21. Input conductance as a function of real frequency, $\Omega = 12.0$ (compared with results of King & Harrison [2]).

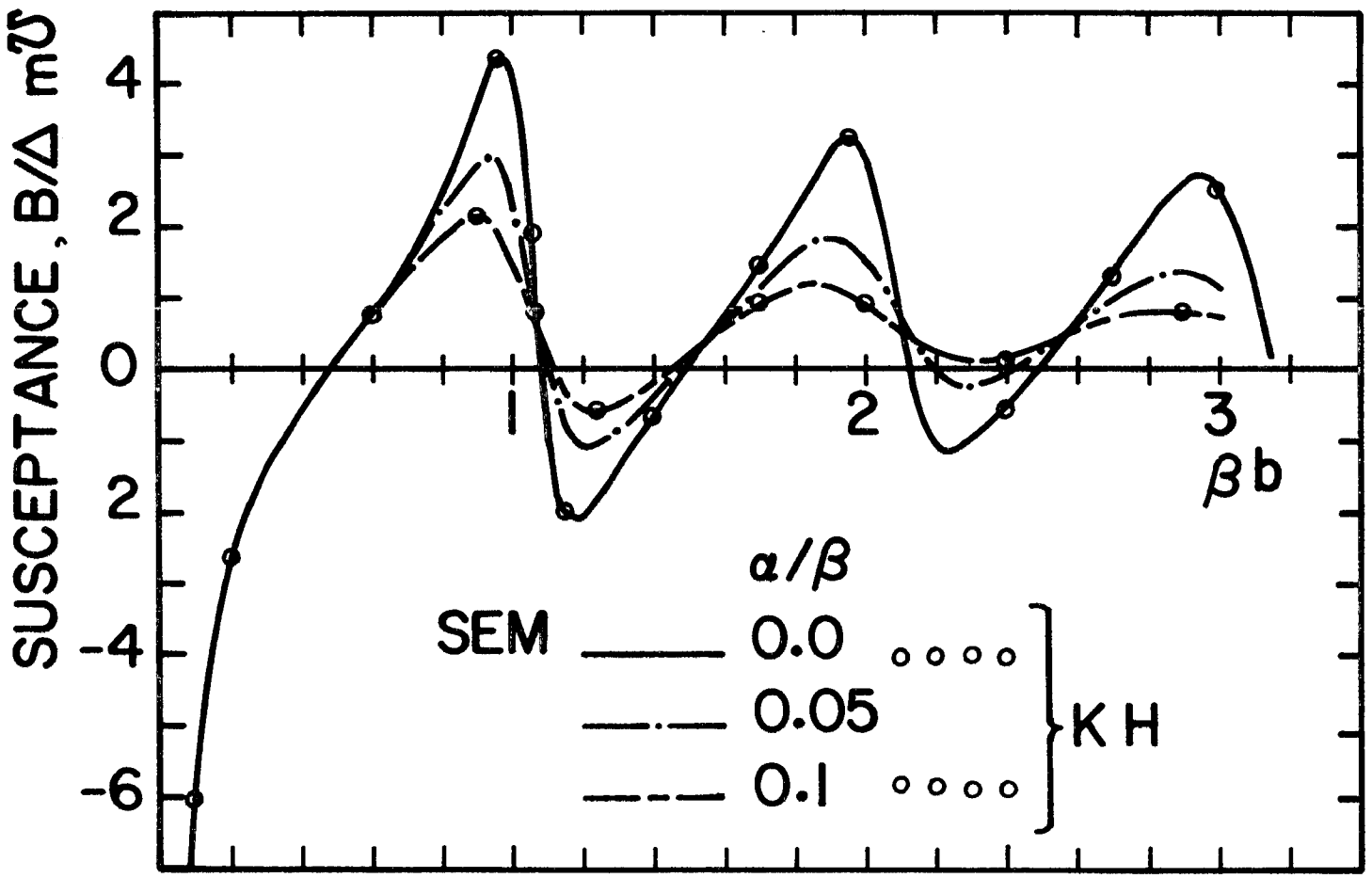

Figure 22. Input susceptance as a function of real frequency, $\Omega = 12.0$ (compared with results of King & Harrison [2]).

$\ell = 3$ and their complex conjugate pairs. We note that for a given ratio of α/β, the corresponding values of γ used simply lie along a radial line from the origin of the γ-plane as shown in Figure 20.

In computing time domain currents for a given normalized conductivity A, one notes that the poles in the s-plane are shifted to new locations which may be found by solving (equation 50) for s and retaining root which approaches the lossless case for A = 0. Figure 23 shows the trajectories of a few of the poles closest to the $j\omega$-axis as a function of A in the s-plane. As A increases, poles move away from the $j\omega$-axis almost parallel to the σ-axis. Hence the principal effect of the lossy medium is to increase the damping constant of all the resonances. The pole at the origin shifts to the left end of the branch cut.

The time domain current is shown in Figure 24, for a pulse excitation at the gap ($\phi = 0$) at $t = 0$ and observed at $\phi = 90°$ on the loop. The pulse width is $c\tau/\pi b = 0.5$. It is interesting to note that as time increases all the curves approach the same constant value and as the magnitude of A increases the current response quickly approaches the final value.

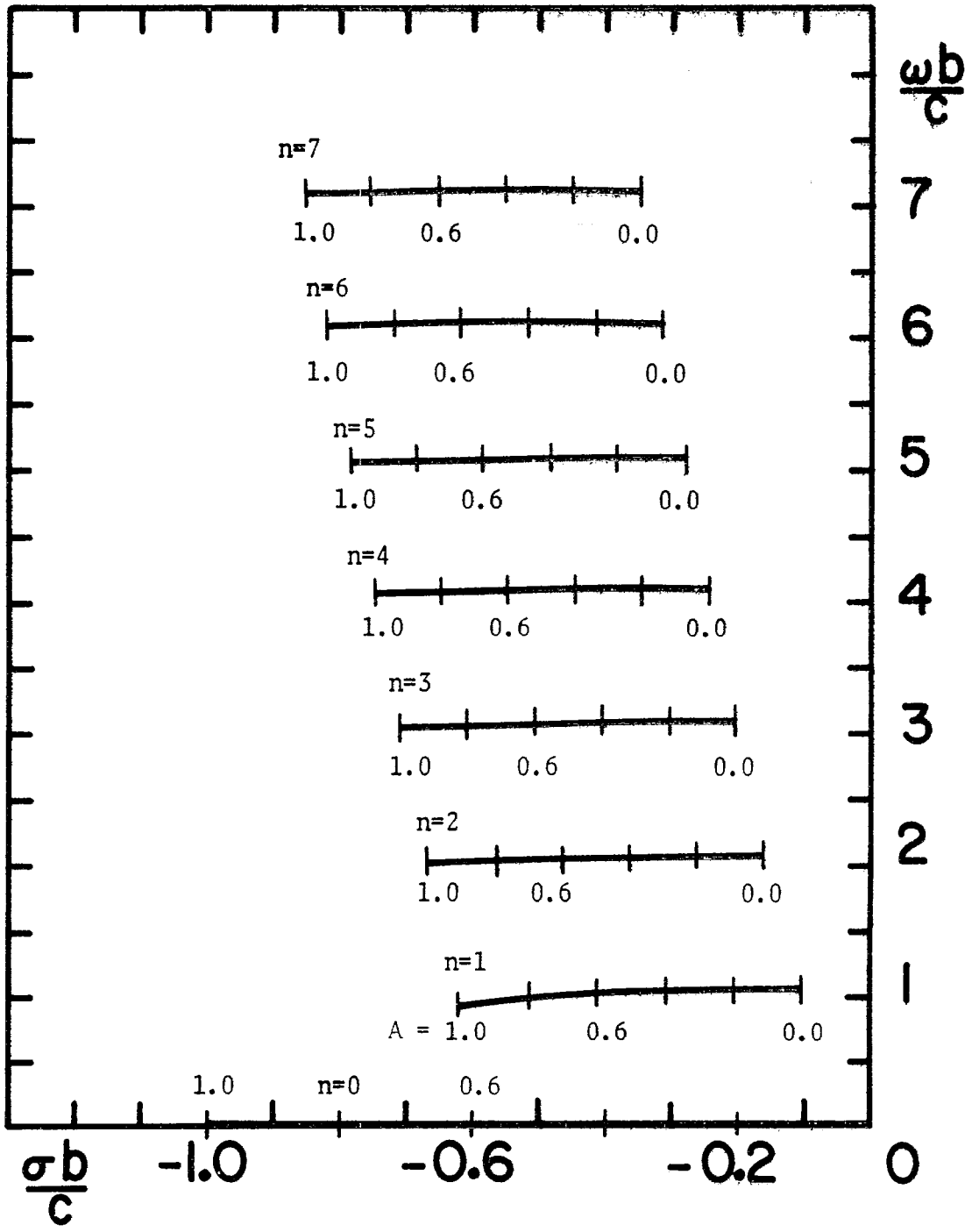

Figure 23. Trajectories of the poles closest to jω-axis as a function of normalized conductivity A.

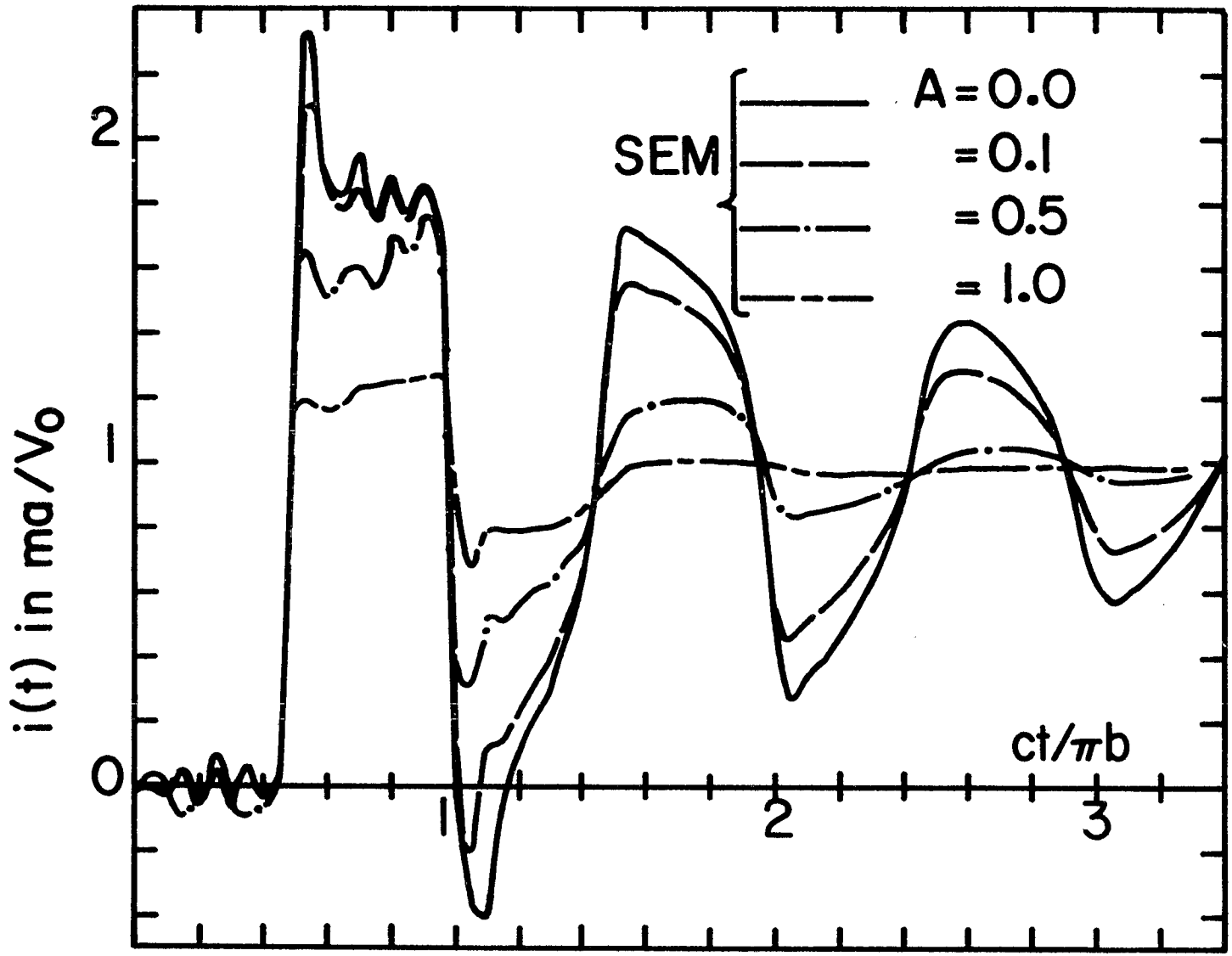

Figure 24. Time domain current in lossy medium, pulse excitation, turn on at t = 0, ϕ = 0 and observed at ϕ = 90°, pulse width $c\tau/\pi b$ = 0.5.

APPENDIX A

ASYMPTOTIC FORM FOR $a_n(s)$

The induced current distribution on the circular loop structure is given by the series expression

$$I(\phi,s) = \sum_{n=-\infty}^{+\infty} I_n(s)e^{-jn\phi} \tag{1A}$$

where the current coefficients are given by

$$I_n(s) = \frac{F_n(s)}{a_n(s)} \tag{2A}$$

$F_n(s)$ are the components of the input excitation coupling to the n-th mode and $a_n(s)$ are the corresponding Fourier coefficients in the series expansion (13). With the substitution

$$\frac{s}{c} = jk \tag{3A}$$

$$a_n(k) = \frac{kb}{2}[K_{n+1} + K_{n-1}] - \frac{n^2}{kb} K_n \tag{4A}$$

and

$$K_0 = \frac{1}{\pi} \ln \frac{8b}{a} - S_0(2kb) \tag{5A}$$

$$K_n = K_{-n} = \frac{1}{\pi}[\mathcal{K}_0(\frac{na}{b})\mathcal{I}_0(\frac{na}{b}) + C_n] - S_{2n}(2kb) \tag{6A}$$

$$S_{2n}(2kb) = +\frac{1}{2}\int_0^{2kb}[\Omega_{2n}(z) + jJ_{2n}(z)]dz \tag{7A}$$

$$C_n = \gamma_e + \ell n(4n) - 2\sum_{m=0}^{n-1}\frac{1}{2m+1} \tag{8A}$$

γ_e: Euler's constant = 0.5772 ...

where $J_{2n}(z)$ and $\Omega_{2n}(z)$ are the complex Bessel and Lommel-Weber functions of order 2n and similarly in the expression (6D), $\mathcal{K}_0$ and $\mathcal{I}_0$ are the modified Bessel functions of zero order respectively. These functions are extensively tabulated in [3] for real arguments. For complex arguments a convenient algorithm [5] is used to generate these functions wherein the accuracy of the evaluation is tested by using their associated wronskians.

The expressions for K_n (14, 15) defined in Section 1 are different from the ones defined in equations (6A, 7A). In fact this has been verified numerically for thin wire circular loop structures, both give same results accuracte up to seven or eight decimal places.

In the following an asymptotic expression for $a_n(s)$ is developed which is essential in the application of SEM. According to the equation (7A)

$$S_m(z) = \frac{j}{2}\int_0^{2z}[J_m(\xi) + jE_m(\xi)]d\xi \tag{9A}$$

where the Weber function $E_m(\xi) = -\Omega_m(\xi)$ (10A)

The asymptotic forms of the integrand of (10A) can be found in [4]

$$J_m(\xi) + jE_m(\xi) \sim J_m(\xi) - jY_m(\xi) - j\frac{1+(-1)^m}{\pi\xi} + O(\frac{1}{\xi^2})$$

$$\sim \sqrt{\frac{2}{\pi\xi}}\, e^{-j[\xi-\frac{1}{2}m\pi-\frac{\pi}{4}]} - j[\frac{1+(-1)^m}{\pi\xi}] \qquad (11A)$$

$$|\arg \xi| < \pi$$

Because of the presence of the term involving $1/\xi$, the integral expression (10A) is not convergent as $z\to\infty$ for even values of m. But it is convergent for odd values of m as is seen by comparing the integral (10A) to the Fresnel types of integrals [3]. However, we make the following rearrangement by splitting the integration limits and adding and subtracting the term involving $1/\xi$ within the integrand

$$S_m(z) = \frac{j}{2}\int_0^1 \left[J_m(\xi) + jE_m(\xi)\right] d\xi + \frac{j}{2}\int_1^{2z} \left[J_m(\xi) + jE_m(\xi)\right.$$

$$\left. + j\frac{1+(-1)^m}{\pi\xi}\right] d\xi + \frac{1+(-1)^m}{2\pi} \ln 2z \qquad (12A)$$

With this rearrangement the second integral is convergent as $z\to\infty$ and hence can be written in the form

$$\frac{j}{2}\int_1^{2z}\left[J_m(\xi) + jE_m(\xi) + j\frac{1+(-1)^m}{\pi\xi}\right] d\xi$$

$$= \frac{j}{2}\left[\int_1^{\infty} + \int_{\infty}^{2z}\right]\left[J_m(\xi) + jE_m(\xi) + j\frac{1+(-1)^m}{\pi\xi}\right] d\xi \qquad (13A)$$

For large z, the integrand in the second integral may be replaced by its asymptotic form (11A) and integrated term by term

$$I = \frac{j}{2}\int_{\infty}^{2z}\left[J_m(\xi) + jE_m(\xi) + j\frac{1+(-1)^m}{\pi\xi}\right]d\xi$$

$$\sim \frac{j}{2}\int_{\infty}^{2z}\sqrt{\frac{2}{\pi\xi}}\,e^{-j\left[\xi-\frac{1}{2}m\pi-\frac{\pi}{4}\right]}d\xi \quad , \quad |\arg z| < \pi \tag{14A}$$

now changing integration variable $\xi = \frac{\pi}{2}t^2$, and splitting the integration ∞ to $\sqrt{\frac{z}{\pi}}$ by ∞ to 0 and 0 to $2\sqrt{\frac{z}{\pi}}$, we have

$$I \sim \left[-\frac{1}{2} - j\frac{1}{2} + S(2\sqrt{\frac{z}{\pi}}) + jC(2\sqrt{\frac{z}{\pi}})\right]e^{j\left[\frac{m\pi}{2}+\frac{\pi}{4}\right]} \quad , \quad |\arg z| < \pi \tag{15A}$$

where C(z) and S(z) are Fresnel integrals

and

$$\left.\begin{aligned} C(z) &= \int_0^z \cos(\tfrac{\pi}{2}t^2)dt \\ S(z) &= \int_0^z \sin(\tfrac{\pi}{2}t^2)dt \end{aligned}\right\} \tag{16A}$$

as defined in [3], where the following asymptotic forms are given

$$\left.\begin{aligned} C(z) &\sim \frac{1}{2} + \frac{1}{\pi z}\sin(\tfrac{\pi}{2}z^2) + \mathcal{O}(\frac{1}{z^2}) \\ S(z) &\sim \frac{1}{2} - \frac{1}{\pi z}\cos(\tfrac{\pi}{2}z^2) + \mathcal{O}(\frac{1}{z^2}) \end{aligned}\right\} \tag{17A}$$

$$|\arg z| < \frac{\pi}{2}$$

Hence

$$I \sim \frac{-1}{2\sqrt{\pi z}} e^{-j\left[2z - \frac{1}{2}m\pi - \frac{\pi}{4}\right]} \quad , \quad |\arg z| < \frac{\pi}{2} \tag{18A}$$

and using (12A), (13A) and (18A), we may write

$$S_m(z) \sim P_m + \frac{1+(-1)^m}{2\pi} \ln z - \frac{1}{2\sqrt{\pi z}} e^{-j\left[2z - \frac{1}{2}m\pi - \frac{\pi}{4}\right]} \quad , \quad |\arg z| < \pi \tag{19A}$$

where P_m is a constant,

$$P_m = \frac{j}{2}\int_0^1 \left[J_m(\xi) + jE_m(\xi)\right]d\xi + \frac{j}{2}\int_1^\infty \left[J_m(\xi) + jE_m(\xi) + j\frac{1+(-1)^m}{\pi\xi}\right]d\xi + \frac{1+(-1)^m}{2\pi} \ln 2 \tag{20A}$$

To evaluate the constant P_m consider (from the equation 19A)

$$P_m = \lim_{z\to\infty}\left[S_m(z) - \frac{1+(-1)^m}{2\pi} \ln z\right] \tag{21A}$$

Therefore

$$P_{m-2} = \lim_{z\to\infty}\left[S_{m-2}(z) - \frac{1+(-1)^{m-2}}{2\pi} \ln z\right] \tag{22A}$$

Substracting (22D) from equation (21D)

$$P_m - P_{m-2} = \lim_{z\to\infty}\left[S_m(z) - S_{m-2}(z)\right] \tag{23A}$$

According to equation (9A)

$$S_m(z) = \frac{j}{2}\int_0^{2z}\left[\frac{1}{\pi}\int_0^{\pi} e^{j[m\theta - \xi \sin\theta]}d\theta\right]d\xi \qquad (24A)$$

Hence by (24A) the bracketed term in the equation (23A) becomes the recurrence relationship

$$S_{m+1}(z) - S_{m-1}(z) = -j[J_m(2z) + jE_m(2z)] - \frac{1-(-1)^m}{m\pi} \qquad (25A)$$

Substituting m = m-1 in (25A) and taking its limit as $z\to\infty$

$$P_m - P_{m-2} = -\frac{1-(-1)^{m-1}}{(m-1)\pi} \qquad (26A)$$

Further rearranging the terms of P_m in the expression (20A) and noting [2]

$$\int_0^{\infty} J_m(\xi)d\xi = 1,$$

$$P_m = \frac{j}{2} - \lim_{z\to\infty}\left[\frac{1}{2}\int_0^{z} E_m(\xi)d\xi + \frac{1+(-1)^m}{2\pi}\,\ell n\, z\right] \qquad (27A)$$

which gives for m = 0 and m = 1, [22]

$$P_0 = \frac{j}{2} - \frac{1}{\pi}\psi\left(\frac{1}{2}\right)$$

$$\text{and} \quad P_1 = \frac{j}{2} \qquad (28A)$$

This leads us directly to write down the general m-th term

$$P_m = \frac{j}{2} - \frac{1+(-1)^m}{2\pi}\,\psi\left(\frac{m+1}{2}\right) \tag{29A}$$

where

$$\psi\left(\frac{1}{2}\right) = -\gamma_e - 2\,\ell n\,2$$

$$\psi(m+1) = \psi(m) + \frac{1}{m}$$

We note further the constant p_m given by equation (20A) indeed satisfies the equation (26A). From (29 A)

$$P_{m-2} = \frac{j}{2} - \frac{1+(-1)^{m-2}}{2\pi}\,\psi\left(\frac{m-1}{2}\right) \tag{30A}$$

subtracting (30A) from equation (29A) in fact gives equation (26A). Thus from equations (19A), (20A) and (29A), the asymptotic formula valid in the region $|\arg z| < \pi$ of the complex plane is given by

$$S_m(z) \sim \frac{j}{2} + \frac{1+(-1)^m}{2\pi}\left[\ell n\, z - \psi\left(\frac{m+1}{2}\right)\right] - \frac{1}{2\sqrt{\pi z}}\, e^{-j\left[2z - \frac{1}{2}m\pi - \frac{\pi}{4}\right]} \qquad |\arg z| < \pi, \tag{31A}$$

The analyticity of $S_m(z)$ ensures that the above asymptotic formula can be continued onto any desired sheet in the complex plane.

With this formula for $S_m(z)$, we are now ready to consider the terms $a_n(kb)$ defined in the expressions (4A) to (7A). Note that for n small and a/b very small, the term

$$\frac{1}{\pi}\left[\mathcal{K}_0\left(\frac{na}{b}\right)\mathcal{J}_0\left(\frac{na}{b}\right) + C_n\right] \sim \frac{1}{\pi}\left[\ell n\frac{8b}{a} - 2\sum_{m=0}^{n-1}\frac{1}{2m+1}\right] \tag{32A}$$

which is just the first term of K_0 if the sum is equal to zero when the upper index is negative. Asymptotically, this becomes

$$K_0 = \frac{1}{\pi}\left[\ell n\frac{2b}{a} - \gamma_e - \ell nkb\right] - \frac{j}{2} + \frac{1}{2\sqrt{\pi kb}}\, e^{j[\frac{\pi}{4} - 2kb]} \tag{33A}$$

$$K_n = K_{-n} = \frac{1}{\pi}[\mathcal{K}_0(\tfrac{na}{b})\mathcal{I}_0(\tfrac{na}{b}) + \ell n\, n - \ell n\, kb]$$

$$- \frac{j}{2} + \frac{(-1)^n}{2\sqrt{\pi kb}}\, e^{j[\frac{\pi}{4} - 2kb]} \tag{34A}$$

where we have made use of the relationship from (31A),

$$S_{2n} \sim \frac{j}{2} + \frac{1}{\pi}[\ell nkb - \psi(n+\tfrac{1}{2})] - \frac{(-1)^n}{2\sqrt{\pi kb}}\, e^{j[\frac{\pi}{4} - 2kb]} \tag{35A}$$

Note that

$$\mathcal{K}_0(\tfrac{na}{b})\mathcal{I}_0(\tfrac{na}{b}) + \ell n\, n \cong -\ell n\,\frac{na}{2b} - \gamma_e + \ell n\, n \cong \ell n\,\frac{2b}{a} - \gamma_e$$

which is a useful approximation for small na/b and shows that

$$K_0 = \lim_{n\to 0} K_n \tag{36A}$$

For kb large, the last term in expression (4A) or a_n

$$a_n = \frac{kb}{2}[K_{n+1} + K_{n-1}] - \frac{n^2}{kb} K_n$$

may be neglected since it is of order 1/kb and the first term is of order kb. Hence

$$a_0 \sim \frac{kb}{\pi}\left[\mathcal{K}_0\left(\frac{a}{b}\right)\mathcal{J}_0\left(\frac{a}{b}\right) - \ell n kb - j\frac{\pi}{2} - \frac{1}{2}\sqrt{\frac{\pi}{kb}}\, e^{j\left[\frac{\pi}{4} - 2kb\right]}\right] \tag{37A}$$

$$a_1 \sim \frac{kb}{2\pi}\left[\ell n\, \frac{2b}{a} - \gamma_e + \mathcal{K}_0\left(\frac{2a}{b}\right)\mathcal{J}_0\left(\frac{2a}{b}\right) + \ell n\, 2 - 2\, \ell n\, kb - j\pi + \sqrt{\frac{\pi}{kb}}\, e^{j\left[\frac{\pi}{4} - 2kb\right]}\right] \tag{38A}$$

and

$$a_n \sim \frac{kb}{2\pi}\left[\mathcal{K}_0\left[\frac{(n-1)a}{b}\right]\mathcal{J}_0\left[\frac{(n-1)a}{b}\right] + \mathcal{K}_0\left[\frac{(n+1)a}{b}\right]\mathcal{J}_0\left[\frac{(n+1)a}{b}\right] + \ell n(n^2-1) - 2\, \ell n kb - j\pi + (-1)^{n+1}\sqrt{\frac{\pi}{kb}}\, e^{j\left[\frac{\pi}{4} - 2kb\right]}\right] \tag{39A}$$

$$|\arg z| < \pi$$

For $\frac{(n-1)a}{b}$, $\frac{(n+1)a}{b}$ small, the latter can be written as

$$a_n \sim \frac{kb}{2\pi}\left[2\, \ell n\, \frac{2b}{a} - 2\gamma_e - 2\, \ell n kb - j\pi + (-1)^{n+1}\sqrt{\frac{\pi}{kb}}\, e^{j\left[\frac{\pi}{4} - 2kb\right]}\right] \tag{40A}$$

A-1 Roots for large values of kb

The roots of a_n for large values of kb may be found by setting the term in the brackets of the expression (3A) equal to zero and rearranging the terms to solve for kb in the exponent,

$$kb = \frac{\pi}{8} + \frac{j}{2}\, \ell n\left[(-1)^n\sqrt{\frac{kb}{\pi}}\,[2\, \ell n\, \frac{2b}{a} - 2\gamma_e - 2\, \ell n kb - j\pi]\right] \tag{41A}$$

Note that there are only two sets of roots, those for n even and those

for n odd. Furthermore, one has to be careful about which branch of the outside logarithm is used in the calculation. This formula is relatively insensitive to kb on the right hand side (because it appears only as ℓnkb and $\sqrt{kb}$, both slowly varying functions) and hence should be highly suitable for calculating kb by iteration. A guess of kb may be inserted in the right hand side to generate an improved value. If the above formula is written as

$$kb = f(kb) \tag{42A}$$

then the iterative algorithm is

$$k_1 b = f(k_0 b),$$

$$k_2 b = f(k_1 b), \ldots\ldots\ldots$$

where $k_0 b$ is the initial guess. The iteration is carried out until it converges.

A-2 Asymptotic formula for residues of $1/a_n(s)$

At zeros of a_n, we have

$$a_n(kb) = \frac{k_{ni} b}{2}\left[K_{n+1}(k_{ni} b) + K_{n-1}(k_{ni} b)\right] - \frac{n^2}{k_{ni} b} K_n(k_{ni} b) = 0 \tag{43A}$$

where k_{ni} is a complex zero of a_n. Thus $1/a_n$ has a (simple) pole when a_n has a (simple) zero. The residue can then be written as

$$\lim_{k \to k_{ni}} (k-k_{ni}) \frac{1}{a_n(kb)} = \left.\frac{1}{\frac{da_n}{dk}}\right|_{k=k_{ni}} \tag{44A}$$

More precisely, we wish to find the residue

$$\lim_{s \to s_{ni}} (s - s_{ni}) \frac{1}{a_n(s)} = \left. \frac{1}{\frac{da_n}{ds}} \right|_{s=s_{ni}} \tag{45A}$$

where $s = jkc$, but this can be found simply by noting that

$$\frac{d}{ds} = -\frac{j}{c} \frac{d}{dk} \tag{46A}$$

From the expressions (34A) and (42A), for large $k = k_{ni}$, K_n' behaves like

$$K_n'(k_{ni}b) = \left. \frac{dK_n}{dk} \right|_{k=k_{ni}} \sim -jb \left[(-1)^n \sqrt{\frac{1}{\pi k_{ni} b}}\, e^{j[\frac{\pi}{4} - 2k_{ni}b]} - \frac{j}{\pi k_{ni} b} \right] \tag{47A}$$

thus the residue is

$$R_{ni} = \left[jb^2 (-1)^n \sqrt{\frac{k_{ni}}{\pi b}}\, e^{j[\frac{\pi}{4} - 2k_{ni}b]} \right]^{-1} \tag{48A}$$

If we are able to form a residue series of the form

$$\sum_i \frac{R_{ni}}{k - k_{ni}} \tag{49A}$$

where

$$R_{ni} = \left. \frac{1}{\frac{da_n}{dk}} \right|_{k=k_{ni}} \tag{50A}$$

and if the poles $k = k_{ni}$ behave approximately like

$$\frac{1}{k_{ni}} = \mathcal{O}\left(\frac{1}{n}\right) \tag{51A}$$

Then the residue series terms

$$\frac{R_{ni}}{k-k_{ni}} = \mathcal{O}(n^{-3/2}) \tag{52A}$$

which is a convergent series.

A-3 Expansion of $1/a_n(s)$ in a residue series

Let us consider $a_n(s)$ in the $s = jkc$ plane. Examination of the asymptotic behavior of the poles (both numerically and observing the asymptotic form of $a_n(s)$), we form the approximate picture below (Figure 1A) of the pole distribution with poles at $\xi = s_{ni}$.

We shall draw a circular contour centered at the origin and passing between two poles as shown. Now consider the following contour integral in the ξ-plane

$$\frac{1}{2\pi j} \oint_{C_n} \frac{d\xi}{\xi^p(\xi-s)a_m(\xi)} \tag{53A}$$

and depending on the nature of the behavior $a_m(\xi)$, the value of the exponent p is selected. For the present problem we chose $p = 0$ and since $a_m^{-1}(\xi) = \mathcal{O}\left(\frac{1}{\xi}\right)$ for ξ on C_n, according to the asymptotic formula the integrand is $\mathcal{O}(\xi^{-2})$ and hence

$$\lim_{n\to\infty} \frac{1}{2\pi j} \oint_{C_n} \frac{d\xi}{(\xi-s)a_m(\xi)} = 0 \tag{54A}$$

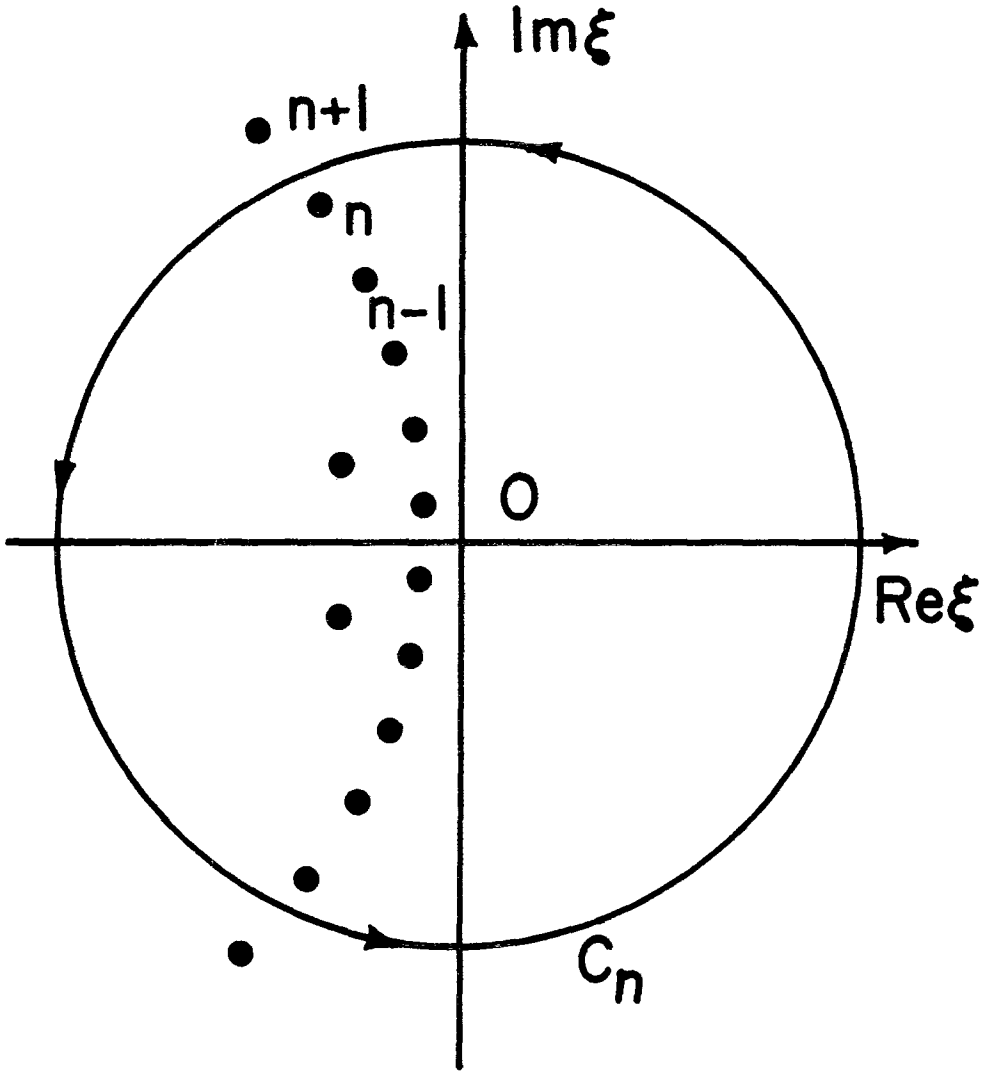

Figure 1A. Contour C_n in complex ξ-plane.

But the integral is also the sum of the residues of the integrand, which yields

$$\frac{1}{a_n(s)} + \sum_i \frac{1}{s_{ni}-s} \lim_{s \to s_{ni}} \frac{s-s_{ni}}{a_n(s)} = 0 \tag{55A}$$

or

$$\frac{1}{a_n(s)} = \sum_i \frac{R_{ni}}{s-s_{ni}} \tag{56A}$$

where R_{ni} is residue of $1/a_n(s)$.

Acknowledgment

The authors would like to thank Maj. R. F. Blackburn for his assistance during the course of this work.

REFERENCES

[1] T. T. Wu, "Theory of Thin Circular Antenna," J. Math. Phys., Vol. 3, pp. 1301-1304, November-December 1962.

[2] R. W. P. King and C. W. Harrison, "The Admittance of Bare Circular Loop Antennas in Dissipative Medium," IEEE Trans. on Antennas and Propagation, Vol. 12, pp. 434-438, March 1964.

[3] M. Abramowitz and A. Stegun, Handbook of Mathematical Functions, Dover, New York, 1964.

[4] G. N. Watson, A Treatise on the Theory of Bessel Functions, Camb. Univ. Press, London, 1966.

[5] J. E. Lewis, "Generation of Bessel Functions of Complex Order and Argument," Electronics Letters, Vol. 7, No. 20, pp. 615-616, October 1971.